7638–7653 *Nucleic Acids Research, 2009, Vol. 37, No. 22* *Published online 30 September 2009*
doi:10.1093/nar/gkp775

Investigation of catalysis by bacterial RNase P via LNA and other modifications at the scissile phosphodiester

Simona Cuzic-Feltens, Michael H. W. Weber and Roland K. Hartmann*

Institut für Pharmazeutische Chemie, Philipps-Universität Marburg, Marbacher Weg 6, D-35037 Marburg, Germany

Received July 13, 2009; Revised August 31, 2009; Accepted September 2, 2009

ABSTRACT

We analyzed cleavage of precursor tRNAs with an LNA, 2′-OCH_3, 2′-H or 2′-F modification at the canonical (c_0) site by bacterial RNase P. We infer that the major function of the 2′-substituent at nt −1 during substrate ground state binding is to accept an H-bond. Cleavage of the LNA substrate at the c_0 site by *Escherichia coli* RNase P RNA demonstrated that the transition state for cleavage can in principle be achieved with a locked C3′ -*endo* ribose and without the H-bond donor function of the 2′-substituent. LNA and 2′-OCH_3 suppressed processing at the major aberrant m_{-1} site; instead, the m_{+1} (nt +1/+2) site was utilized. For the LNA variant, parallel pathways leading to cleavage at the c_0 and m_{+1} sites had different pH profiles, with a higher Mg^{2+} requirement for c_0 versus m_{+1} cleavage. The strong catalytic defect for LNA and 2′-OCH_3 supports a model where the extra methylene (LNA) or methyl group (2′-OCH_3) causes a steric interference with a nearby bound catalytic Mg^{2+} during its recoordination on the way to the transition state for cleavage. The presence of the protein cofactor suppressed the ground state binding defects, but not the catalytic defects.

INTRODUCTION

Endonucleolytic 5′-end maturation of tRNA primary transcripts is catalyzed by the ribonucleoprotein enzyme Ribonuclease P (RNase P) in all three domains of life (Archaea, Bacteria and Eukarya) as well as in mitochondria and chloroplasts (1–4). An exception is the human mitochondrial tRNA 5′-end maturation enzyme that lacks an RNA subunit, with its three protein subunits recruited from related and unrelated biochemical pathways (5). Bacterial RNase P enzymes are composed of a catalytic RNA subunit (6), ∼400 nucleotides (nt) in length, and a single small protein of typically 120 amino acids (7). The protein is essential *in vivo*, but *in vitro* its absence can be compensated by increased mono- and particularly di-valent cations (6). Studies with RNase P RNA ribozymes (P RNAs) from *Escherichia coli* and *Bacillus subtilis* have indicated a specific role for at least two metal ions in productive enzyme–substrate complex formation and cleavage chemistry (8–15). Since processing of precursor tRNAs (ptRNAs) by RNase P results in cleavage products with 3′-OH and 5′-phosphate termini, an inherent feature of RNase P catalysis must be to prevent the 2′-hydroxyl group at the cleavage site from attacking the scissile phosphodiester, which would otherwise result in 5′-OH and 2′,3′-cyclic phosphate ends. The 2′-hydroxyl group of the ribose at the cleavage site has indeed been identified as being crucial in the catalytic process. A 2′-deoxy or 2′-amino substitution at the canonical RNase P cleavage site (nt −1) affected substrate ground state binding, cleavage site recognition, binding of catalytically important Mg^{2+} and substantially reduced the cleavage rate by *E. coli* or *B. subtilis* P RNA (8,16–23). Initial evidence for the 2′-hydroxyl group at nt −1 acting as a ligand for a catalytic Mg^{2+} ion came from the observation that a 2′-deoxy modification at this location reduced the Hill coefficient for the Mg^{2+} dependence of substrate cleavage from 3 to 2 and increased the apparent K_d for Mg^{2+} binding 10^3-fold (8). A 2′-amino modification at this position resulted in miscleavage at lower pH, consistent with the idea that protonation of the 2′-amino group at lower pH causes electrostatic repulsion of a metal at this location (20,21). Mn^{2+} rescued cleavage at the canonical c_0 site for ptRNA with a 2′-amino substitution at nt −1, which would be consistent with a direct metal ion coordination to the 2′-substituent at this location; however, a 2′-deoxy modification at the same site was rescued to a similar extent by Mn^{2+}, thus questioning the possibility of a direct metal

*To whom correspondence should be addressed. Tel: +49 6421 2825827; Fax +49 6421 2825854; Email: roland.hartmann@staff.uni-marburg.de
Present address:
Dr Simona Cuzic-Feltens, Martin-Luther Universität Halle, Institut für Biochemie und Biotechnologie, Kurt-Mothes Strasse, 306120 Halle (Saale), Germany.

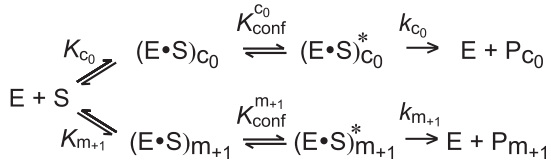

Scheme 1. Model for parallel cleavage pathways under single turnover conditions, modified based on previous models (24,51). In this example, aberrant cleavage occurs at the m_{+1} site. Rapid equilibria of $(E\bullet S)c_0$ and $(E\bullet S)m_{+1}$ commit the complexes to reaction along the different pathways. Before the bond breakage (k_{c_0} and $k_{m_{+1}}$), $(E\bullet S)c_0$ and $(E\bullet S)m_{+1}$ complexes are assumed to undergo a conformational rearrangement (E•S -> E•S*).

contact (20). We rather favor the concept of the 2′-OH at nt −1 interacting with a water molecule from the hydration shell of this metal ion (8,20). Pan and coworkers found that a 2′-deoxy substitution at the c_0 cleavage site had a large effect on ptRNA cleavage by *B. subtilis* P RNA, whereas two *in vitro* selected non-tRNA substrates were little affected by such a substitution at the cleavage site; rather, the 2′-OH one nucleotide upstream was identified to be critical for cleavage of these non-tRNA substrates which lack a T stem-loop module (24). They inferred a model according to which a unique 2′-OH near the cleavage site favors a concentration-independent conformational rearrangement or docking step of initial E•S complexes [(E•S) → (E•S)*; Scheme 1] that precedes the catalytic step. This unique 2′-OH is usually the one at the c_0 site in the case of ptRNAs that are able to form the T stem-loop interaction with the P RNA S domain, but another 2′-OH in the vicinity may be utilized to fulfill this role in the absence of the T stem-loop interaction. In addition, the P protein shifts the equilibrium towards (E•S)*, thus often mitigating defects of the P RNA-alone reaction which are due to impaired (E•S)* formation. Based on this model, the 2′-OH at the c_0 site in ptRNA substrates likely affects K_{conf} of the docking step as well as catalysis (k_{c_0}; Scheme 1).

NMR experiments have indicated that the metal ion coordinated with the help of the 2′-OH group at nt −1 is actually 'prebound' to ptRNA before complexation with P RNA (25). In a related study, the ribose at nt −1, if not involved in base pairing, was found to be predominantly 2′-*endo* puckered (26), raising the possibility that a C2′-*endo* sugar pucker may be the favored conformation in the transition state after potential –1/73 base pairs have been disrupted through formation of the +73/294 interaction with P RNA (27). To address the role of sugar conformation at the cleavage site for the catalytic process, we analyzed a ptRNA with a locked nucleic acid (LNA) substitution at nt −1, which arrests the ribose in a C3′-*endo* pucker (28,29) (Figure 1). For better evaluation of effects caused by the locked ribose conformation, the loss of the H-bond donor function at the 2′-oxygen and sterical impediments due to the presence of an additional methylene group, the ptRNA variant with a 2′-OCH_3 modification at this position was included in our analysis. As LNA, the 2′-OCH_3 group can accept but not donate H-bonds. Unlike LNA, the 2′-OCH_3 modified ribose has a flexible conformation (Table 1) and the 2′-OCH_3 group can freely rotate around the C2′–O2′ bond, whereas the position of the corresponding methylene is fixed in LNA. Other variants with 2′-fluoro (2′-F) or 2′-deoxy (2′-H) substitutions at nt −1 that affect the H–bonding pattern, the free energy of solvation and the electronegativity of the 2′–substituent were included as well. We then characterized the modified ptRNA substrates in reactions catalyzed by type A (*E. coli*) and type B (*B. subtilis*) RNase P (RNA) for (i) substrate ground state binding, (ii) cleavage site selection and (iii) cleavage kinetics. Our results indicate that the major function of the 2′–substitutent at nt −1 during substrate ground state binding is to accept an H-bond. We demonstrate that cleavage at the canonical site by *E. coli* P RNA can occur in the presence of a locked C3′-*endo* ribose and without the H-bond donor function of the 2′-substituent, however, with very low efficiency. The strong catalytic defect in the presence of LNA and 2′-OCH_3 modifications at the c_0 site supports a model where the extra methylene (LNA) or methyl group (2′-OCH_3) causes a steric interference with a nearby bound catalytic Mg^{2+} during its recoordination on the way to the transition state for cleavage. LNA and 2′-OCH_3 at the c_0 site also suppressed processing at the major aberrant m_{-1} site, directing cleavage to the aberrant m_{+1} site (nt +1/+2). The protein cofactor, although suppressing the ground state binding defects, was unable to substantially relieve the severe catalytic defects. Differences between *E. coli* and *B. subtilis* enzymes included a stronger defect caused by 2′-H at nt −1 on the *B. subtilis* versus *E. coli* holoenzyme, and different cleavage site selection on the 2′-OCH_3 substrate.

MATERIALS AND METHODS

RNA synthesis, 5′-phosphorylation of RNA, 5′-end-labeling of RNA and assembly of ptRNA variants

Chemical and enzymatic RNA synthesis, purification, 5′-phosphorylation and 5′-^{32}P-end-labeling of RNA, as well as the assembly of ptRNA variants with single-site modifications were performed exactly as described (20,30).

Preparation of recombinant RNase P proteins

E. coli and *B. subtilis* RNase P proteins carrying an N-terminal His-tag were overexpressed and purified as described (31).

Reconstitution of RNase P holoenzymes

(i) For cleavage experiments, a solution containing 133 nM *E. coli* or *B. subtilis* P RNA, 107 mM KCl, 53 mM MES, pH 6.0 and 10.7 mM $MgCl_2$ was incubated for 5 min at 55°C and 50 min at 37°C. To 15 µl of this solution, 1 µl of P protein solution (freshly thawed and diluted) was added to adjust the solution to 0.5 µM *B. subtilis* or 1.2 µM *E. coli* P protein and to 125 nM P RNA, 100 mM KCl, 50 mM MES and 10 mM $MgCl_2$, pH 6.0. This mixture was incubated for another 5 min at 37°C;

16 µl thereof were then combined with 4 µl ptRNA solution (preincubated in the same buffer for 5 min at 55°C and 25 min at 37°C) to start the processing reaction.

(ii) For binding experiments, a solution containing 1.18 µM *E. coli* or *B. subtilis* P RNA, 235 mM NH_4OAc, 59 mM Tris–acetate, pH 7.1, 17.7 mM $CaCl_2$ and 0.059 (w/v) Nonidet P40 was incubated for 1 h at 37°C. To 8.5 µl of this mixture, 1.5 µl of P protein solution was added to adjust the solution to 5 µM *B. subtilis* or 12 µM *E. coli* P protein (freshly thawed and diluted), 1 µM P RNA, 200 mM NH_4OAc, 50 mM Tris–acetate, pH 7.1, 15 mM $CaCl_2$ and 0.05 (w/v) Nonidet P40. This holoenzyme stock solution was incubated for 15 min at 37°C and then used to prepare serial dilutions in the same buffer. The diluted solutions were incubated for another 5 min at 37°C; 10 µl of individual holoenzyme solutions were combined with an equal volume of 5′-^{32}P-labeled ptRNA solution (<1 nM ptRNA, 80 000 Cerenkov cpm), which had been preincubated for 30 min at 37°C in the same buffer, followed by a final incubation step for 5 min at 37°C before conduction of the spin column assay (see below). For cleavage and binding experiments, the final RNase P holoenzyme concentration was considered equal to the final P RNA concentration. This represents an upper estimate of the enzyme concentration, since 100% ribonucleoprotein complex formation may not have been reached.

Nuclease P1 hydrolysis

A solution of 5′-^{32}P-end-labeled 24-mer RNA (10^4 Cerenkov cpm/µl), 0.1 µg/µl carrier RNA, 40 mM NH_4OAc, 0.4 mM $ZnSO_4$, pH 5.3 and 0.01 ng/µl nuclease P1 was incubated for 20 s at 70°C in a heating block. After incubation the reaction tube was placed on ice, the RNA was concentrated and desalted by ethanol precipitation and analyzed by denaturing PAGE.

Kinetics

The ptRNA variants were processed under single turnover conditions at saturating enzyme concentrations (5 µM *E. coli* or *B. subtilis* P RNA or 100 nM of reconstituted *E. coli* or *B. subtilis* RNase P holoenzyme), 1 M NH_4OAc (for RNA-alone reactions) or 0.1 M KCl (for holoenzyme reactions), and at Mg^{2+} concentrations and pH conditions as specified. The pH of 7.0 was chosen to provide conditions where substantial cleavage of all variants occurred, even at low Mg^{2+} concentrations; pH values of 5.5 or 6.0 allowed us to analyze cleavage at rate-limiting chemistry for all substrates (9). All processing reactions were performed at 37°C, P RNA solutions were preincubated for 1 h at 37°C and ptRNA solutions for 5 min at 55°C and 25 min at 37°C before mixing the two. For holoenzyme kinetics, an additional enzyme reconstitution procedure was included (see above). Aliquots withdrawn at different time points from enzyme–substrate mixtures were subjected to ethanol precipitation in the presence of 20 µg of glycogen before analysis by 20% PAGE/8 M urea. Data analysis and calculation of single turnover rate constants of cleavage (k_{obs}) was performed as described (32). For the Mg^{2+} titration experiments in Figure 4E, data were analyzed by non-linear regression analysis using the Hill equation $k_{obs} = k_{obs,\,max} \bullet [Mg^{2+}]^n/(K' + [Mg^{2+}]^n)$.

ptRNA binding by spin column assays

Spin column assays for the determination of equilibrium dissociation constants (K_d) of enzyme–substrate complexes were performed as described (10). Binding of ptRNAs to P RNA was analyzed in a buffer containing 50 mM MES, 1 M NH_4OAc, $CaCl_2$ (15 mM) or $SrCl_2$ (5 or 80 mM), 0.1 % (w/v) SDS, 0.05 % (w/v) Nonidet P40, pH 6.0. Binding of ptRNAs to holoenzymes was analyzed in a buffer containing 50 mM Tris–acetate, 0.2 M NH_4OAc, 15 mM $CaCl_2$, 0.05 % (w/v) Nonidet P40, pH 7.1.

RESULTS

The bacterial ptRNA^{Gly} variants with single modifications at nt −1 were constructed by ligation in the D loop after annealing of a synthetic 24-mer to a 5′-truncated tRNA transcript (Figure 1A). The different 2′-ribose modifications at nt −1 are illustrated in the boxes on the left. Several physico-chemical properties of the 2′-substituents investigated here are summarized in Table 1. The locked C3′-*endo* conformation of an LNA residue is shown in comparison to that of regular nucleotides in Figure 1B. To put our data into a broader perspective, we analyzed the substrates in reactions catalyzed by *E. coli* and *B. subtilis* RNase P (RNA), the main model systems for the two structurally distinct classes of bacterial P RNAs, type A (for 'ancestral') and type B (for 'Bacillus') (33–37).

Effect of modifications at nt −1 on substrate binding by *E. coli* P RNA

Two sets of variants of ptRNA^{Gly} were investigated. The first set carried ribothymidines (rT) at nt −1 and −2 and a 2′-OH, 2′-OCH_3 or LNA modification at nt −1 [referred to as 2′-OH (T-1), 2′-OCH_3 (T-1) and LNA (T-1)] or LNA at nt −2 [LNA (T-2)]. The ribothymidines at positions −1 and −2 were introduced for reasons of comparability with variants carrying LNA substitutions at nt −1 or −2, because LNA analogs for uridine were not available. The second set of substrates carried a C at nt −1 and U at nt −2, and a 2′-OH, 2′-fluoro (2′-F) or 2′-deoxy (2′-H) substituent at position −1 [referred to as 2′-OH (C-1), 2′-F (C-1) and 2′-H (C-1)]. We determined equilibrium dissociation constants (K_d) for binding of ptRNA^{Gly} variants to *E. coli* P RNA at two Sr^{2+} (5 and 80 mM) and one Ca^{2+} (15 mM) concentration (Table 2). Both metal ions support substrate binding to *E. coli* P RNA with similar efficiency as Mg^{2+}, but are inactive (Sr^{2+}) or very inefficient (Ca^{2+}) as catalytic cofactors [(30) and references therein]. The ptRNA with rT residues at −2 and −1, variant 2′-OH (T-1), bound to *E. coli* P RNA with the same affinity (within 2-fold) as the variant with U at −2 and C at −1,

variant 2′-OH (C-1) (Table 2), indicating that the extra methyl groups on the bases as well as the pyrimidine identity at nt −1 had no or very marginal effects on substrate binding in the ground state. This essentially pertains to the LNA (T-2) substrate as well, which differed from the control substrate 2′-OH (T-1) only by a 3–4-fold increase in K_d at the lowest divalent metal ion concentration (5 mM Sr^{2+}). Thus, an LNA modification at nucleotide −2 had little effect on substrate binding by *E. coli* P RNA.

At all three tested metal ion conditions, binding defects were seen for the 2′–F (C-1) (2–4-fold), LNA (T-1) (2–13-fold), 2′-H (C-1) (9–60-fold) and 2′-OCH_3 (T-1) substrate (30–50-fold). Remarkably, the binding defect for LNA (T-1) was essentially suppressed (within 3-fold) at 15 mM Ca^{2+} or 80 mM Sr^{2+} (Table 2). For comparison, the 2′-H (C-1) ptRNA was still bound with 9–11-fold reduced affinity under the same conditions, thus even exceeding the defect of a 2′-F substitution (4-fold effect on K_d). In summary, the LNA substitution at position −1 had only a very minor impact on ptRNA ground state binding, despite its bulky extra methylene group and a sugar pucker arrested in C3′-*endo*. In contrast, the structurally related 2′-OCH_3 modification caused a >30-fold affinity decrease at all tested metal ion concentrations. The 2′-deoxy substitution caused the largest affinity decrease, 60-fold at 5 mM Sr^{2+}, which could be mitigated to 10-fold at the higher divalent metal ion concentrations. From the comparison of an LNA versus 2′-H and 2′-F modification at nt −1 we infer that the presence of a 2′-substituent at nt −1 with good H-bond acceptor capacity, such as the 2′-oxygen, is a major determinant for metal-dependent formation of E–S ground state complexes. Such information could not be extracted from the results obtained with the related 2′-OCH_3 modification, because the steric effect dominates for 2′-OCH_3.

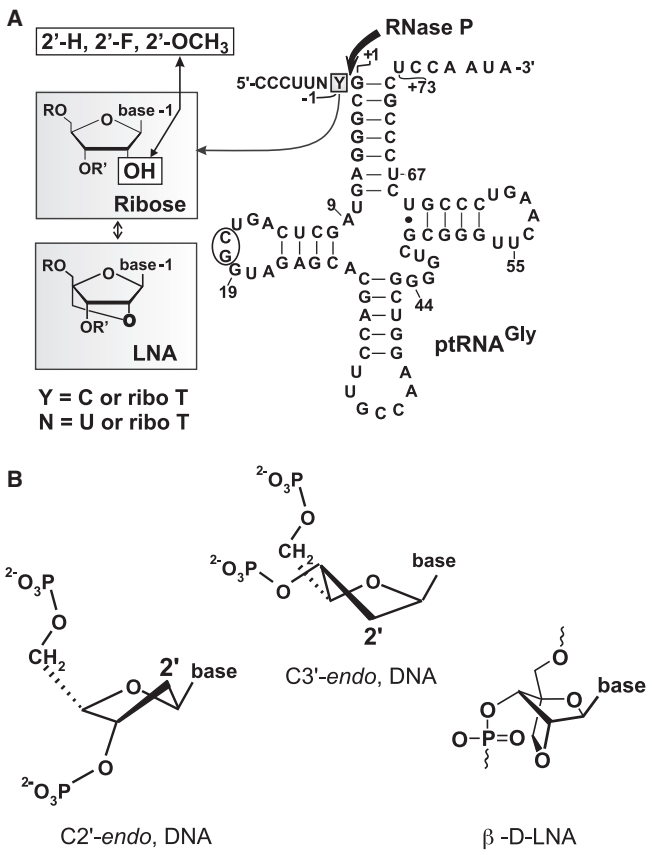

Figure 1. (**A**) Secondary structure of the ptRNA^{Gly} substrate. The modified position (Y, nt −1) at the canonical (c_0) RNase P cleavage site (between nt −1 and +1, marked by the arrow) is boxed. Ribose modifications are illustrated in the grey-shaded boxes on the left. Y at nt −1 represents a C or a ribo T; N at nt −2 stands for U or ribo T. The ligation site in the D-loop used for construction of different ptRNA variants is indicated by the circle. **(B)** Ribose sugar puckers prevailing in natural nucleic acids, from left to right: C2′-*endo* (type S) conformation typical of DNA in B-type helices, C3′-*endo* (type N) conformation typical of A-helical RNA, and the locked C3′-*endo* conformation in LNA; the C2′-*endo* and C3′-*endo* conformers (left and center) are shown with 2′-deoxyribose for clarity reasons.

Effect of modifications at nt -1 on substrate binding by *B. subtilis* P RNA

B. subtilis P RNA bound the control all-ribose substrates at 15 mM Ca^{2+} with 19–26-fold lower affinity than *E. coli* P RNA (Table 2), consistent with previous findings (37). Again, whereas the LNA (T-1) substrate showed little perturbation of substrate binding relative to the 2′-OH (T-1) substrate (2.6-fold increase in K_d), the defect was most pronounced for the substrate with 2′-OCH_3 at −1 (11-fold increase in K_d). Here, the 2′-H substitution reduced affinity only 2-fold and a 2′-F substituent was bound with roughly equal affinity as the 2′-OH (C-1) control substrate. These results are qualitatively similar to those obtained with *E. coli*

Table 1. Some physico-chemical properties of ribose moieties with different 2′-substituents

2′-substituent	H-bond donor	H-bond acceptor	Flexible ribose conformation	Preferentially adopted sugar pucker[a]	Relative solubility[b]	Electronegativity of 2′-substituent	Sterical impediments
2′-OH	Yes	Yes	Yes	C3′-*endo*	Highest	High	No
LNA	No	Yes	No	Locked C3′-*endo*	Intermediate	High	Yes
2′-OCH_3	No	Yes	Yes	C3′-*endo*	Intermediate	High	Yes
2′-H	No	No	Yes	C2′-*endo*	Lowest	Low	No
2′-F	No	Yes	Yes	C3′-*endo*	Low	Highest	No

[a]Information for LNA taken from Petersen *et al.* (52) for conformational equilibria of ribose and 2′-substituted riboses (2′-OH, 2′-H and 2′-OCH_3), see Guschlbauer and Jankowski (53).
[b]According to Cramer and Truhlar (54).

Table 2. Substrate ground state binding to *E. coli* and *B. subtilis* P RNAs and holoenzymes

$[Me^{2+}]$	ptRNA	*E. coli*				*B. subtilis*			
		P RNA		Holoenzyme		P RNA		Holoenzyme	
		K_d (nM)	$K_{d,rel}$	K_d (nM)	$K_{d,rel}$	K_d (nM)	$K_{d,rel}$	K_d (nM)	$K_{d,rel}$
5 mM Sr^{2+}	2′-OH (T-1)	86 ± 22	1.0	–	–	–	–	–	–
	LNA (T-1)	1143 ± 232	13.3	–	–	–	–	–	–
	2′-OCH_3 (T-1)	4168 ± 733	48.5	–	–	–	–	–	–
	LNA (T-2)	295 ± 70	3.4						
	2′-OH (C-1)	48 ± 20	1.0	–	–	–	–	–	–
	2′-F (C-1)	103 ± 49	2.1	–	–	–	–	–	–
	2′-H (C-1)	2887 ± 874	60.1	–	–	–	–	–	–
15 mM Ca^{2+}	2′-OH (T-1)	6.1 ± 2.3	1.0	1.1 ± 0.11	1.0	158 ± 25	1	1.4 ± 0.7	1.0
	LNA (T-1)	15.5 ± 3.7	2.5	1.1 ± 0.34	1.0	418 ± 107	2.6	2.2 ± 0.7	1.6
	2′-OCH_3 (T-1)	191.4 ± 4	31.4	3.8 ± 0.64	3.5	1735 ± 172	11.0	5.7 ± 2	4.1
	LNA (T-2)	6.7 ± 3	1.1						
	2′-OH (C-1)	7.6 ± 1.3	1.0	0.92 ± 0.21	1.0	148 ± 34	1.0	2.1 ± 0.3	1.0
	2′-F (C-1)	27.1 ± 3.7	3.6	1.24 ± 0.35	1.3	178 ± 21	1.2	6.3 ± 0.9	3.0
	2′-H (C-1)	82.5 ± 11.3	10.9	1.9 ± 0.77	2.1	328 ± 69	2.2	12.6 ± 2.8	6.0
80 mM Sr^{2+}	2′-OH (T-1)	5.9 ± 2.9	1.0	–	–	–	–	–	–
	LNA (T-1)	11.5 ± 4.2	1.9	–	–	–	–	–	–
	2′-OCH_3 (T-1)	211 ± 61	35.8	–	–	–	–	–	–
	LNA (T-2)	7.4 ± 2.4	1.25						
	2′-OH (C-1)	7.4 ± 2	1.0	–	–	–	–	–	–
	2′-F (C-1)	29.9 ± 8.3	4.0	–	–	–	–	–	–
	2′-H (C-1)	67.9 ± 16.4	9.2	–	–	–	–	–	–

The analysis of ptRNA binding was performed using the spin column assay (10). The dissociation constant (K_d) was measured in the presence of 50 mM MES/NaOH, pH 6.0, 1 M NH_4OAc (P RNA) and Ca^{2+} (15 mM) or Sr^{2+} (5 or 80 mM) as the divalent metal ion; ptRNA binding to the holoenzyme was assayed at 50 mM Tris/CH_3COOH, 0.2 M NH_4OAc, 15 mM Ca^{2+}, pH 7.1. Relative K_d values ($K_{d,rel}$): individual K_d divided by K_d for the corresponding all-ribose ptRNA. K_d values for the 2′-F (C-1) and 2′-H (C-1) substrates at 15 mM Ca^{2+} are consistent (within 2-fold) with K_d values determined in a previous study under identical conditions (20).

P RNA, except for the generally weaker substrate affinity of *B. subtilis* P RNA and its relatively low apparent sensitivity to the 2′-H substitution at C-1.

Effect of modifications at nt −1 on substrate binding by RNase P holoenzymes

We further investigated binding of the modified substrates to *E. coli* and *B. subtilis* RNase P holoenzymes at 15 mM Ca^{2+} but in the presence of a 5-fold lower monovalent salt concentration (0.2 M) than in RNA-alone assays. The presence of the protein cofactor increased and equalized substrate affinity (K_d values between 1 and 13 nM; Table 2) and abolished the substrate affinity differences seen for *E. coli* relative to *B. subtilis* P RNA. The 2′-H (C−1) ptRNA was exceptional, as it was bound with 6-fold lower affinity than its control substrate by the *B. subtilis* holoenzyme, thus even exceeding the defect of the 2′-OCH_3 (T-1) substrate (3.5-fold for *E. coli*, 4.1-fold for *B. subtilis* RNase P). Thus, a pronounced defect of 2′-H, not evident in the *B. subtilis* P RNA-alone affinity assay, emerged in the holoenzyme context. LNA at nt −1 affected ground state binding to the holoenzymes insignificantly.

Cleavage site selection

Escherichia coli P RNA is known to form alternative E−S complexes in response to structural changes in the enzyme and/or substrate RNA, which lead to aberrant cleavage usually one nucleotide upstream (m_{-1} site, between −2 and −1) of the canonical cleavage site (c_0 site, between −1 and +1) (see e.g. 14,27). More rarely, aberrant cleavage at the m_{+1} site (between nt +1 and +2) has also been observed in reactions catalyzed by *E. coli* and *B. subtilis* P RNA (Figure 2A) (8,19,22).

Except for the LNA (T-1) and 2′-OCH_3 (T-1) substrates, all ptRNA variants listed in Table 2 were processed exclusively at the c_0 site by *E. coli* P RNA (data not shown). The cleavage sites for ptRNA with LNA or 2′-OCH_3 at −1 were analyzed by co-electrophoresis of nuclease P1 hydrolysis ladders (P1 like RNase P generates 5′-phosphate termini) along with the products derived from *E. coli* P RNA cleavage. This revealed cleavage of the LNA (T-1) ptRNA at the c_0 and m_{+1} sites (Figure 2B and C, lanes 2 and 9, respectively), whereas the 2′-OCH_3 (T-1) ptRNA was cleaved exclusively at the m_{+1} site (Figure 2B and C, lanes 4 and 2, respectively). The 7-nt 5′-cleavage product with the 3′-terminal LNA sugar generated by cleavage at the c_0 site (Figure 2B, lane 2) migrated somewhat faster than the corresponding all-ribose counterpart (Figure 2B, lane 6). Changes in the mobility of short oligonucleotides with 3′-terminal ribose modifications in high-resolution gels have been documented before (20,22).

The *E. coli* RNase P holoenzyme cleaved the LNA (T-1) and 2′-OCH_3 (T-1) ptRNAs with very low efficiency relative to the unmodified substrate (Figure 2C, lanes 5

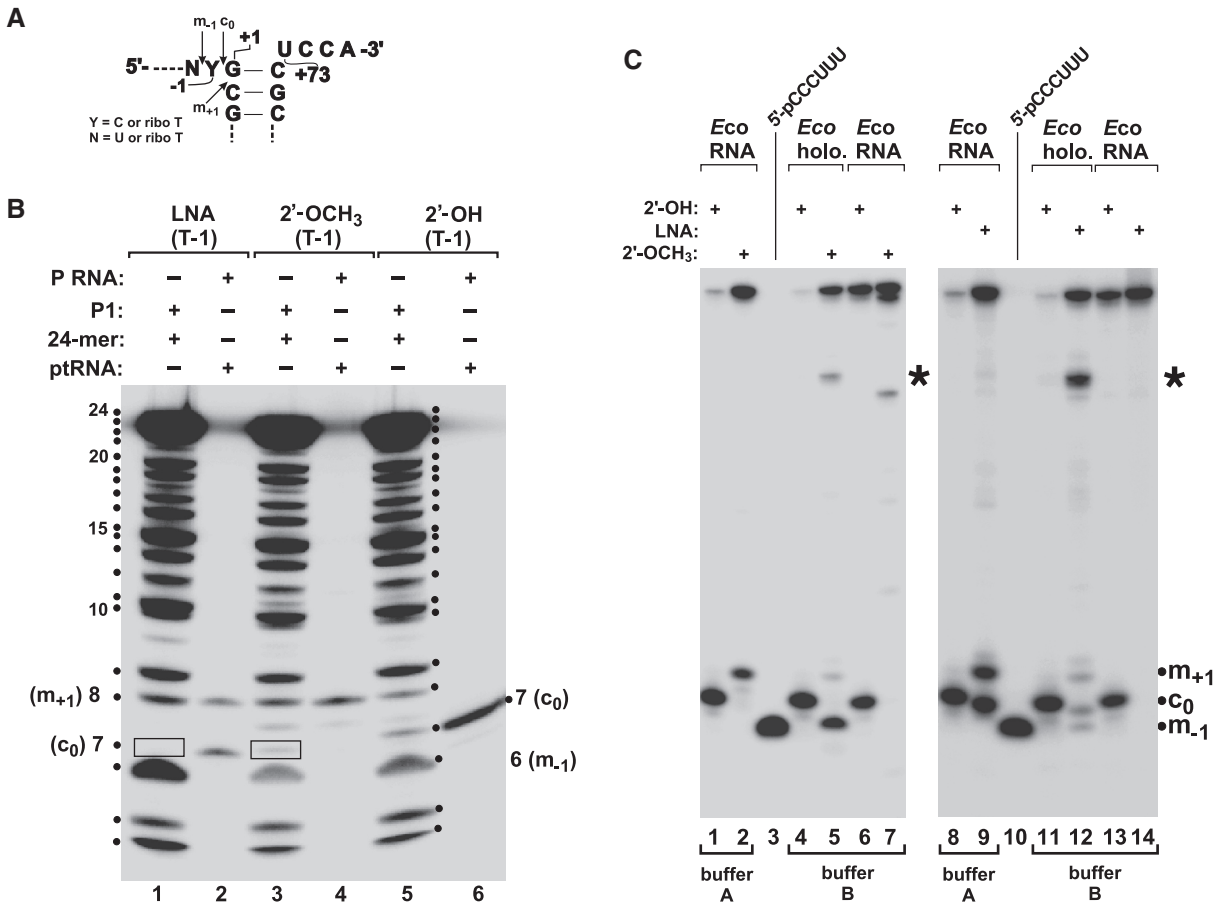

Figure 2. Analysis of RNase P cleavage site selection; (**A**) Secondary structure of ptRNA acceptor stem ends; arrows assign the different RNase P (RNA) cleavage sites: c_0, canonical site; m_{-1}, m_{+1}, aberrant sites. (**B**) Cleavage of ptRNA variants LNA (T-1), 2′-OCH_3 (T-1) and 2′-OH (T-1) by *E. coli* P RNA (lanes 2, 4 and 6) and cleavage of the corresponding 24-mers (Figure 1A) used to construct the ptRNA variants by nuclease P1 (lanes 1, 3 and 5). Numbers on the left side indicate the length (nt) of fragments generated by nuclease P1; the corresponding P RNA cleavage sites are indicated in parentheses. The rectangles mark the missing or reduced P1 fragments due to the absence of a 2′-OH at the corresponding position. Hydrolysis by nuclease P1 was performed as described in the 'Materials and Methods' section. *E. coli* P RNA cleavage was performed in buffer A (1 M NH_4OAc, 50 mM PIPES, pH 7 and 20 mM Mg^{2+}) for 8 h (lane 2), 22 h (lane 4) and 10 min (lane 6) at 37°C. (**C**) Analysis of cleavage site selection by *E. coli* P RNA and holoenzyme. In lanes 1, 2, 8 and 9, processing by *E. coli* P RNA was performed in buffer A as in panel B; cleavage by the *E. coli* holoenzyme (lanes 4, 5, 11 and 12) was conducted in buffer B (50 mM MES, pH 6, 0.1 M KCl and 10 mM $MgCl_2$); we also included control reactions in buffer B in the absence of the *E. coli* protein subunit (lanes 6, 7, 13 and 14), which illustrate the requirement for the protein cofactor under low salt conditions: the LNA and 2′-OCH_3 substrates were cleaved by *E. coli* P RNA in buffer A, but not in buffer B (lanes 2 and 9 versus 7 and 14). The incubation time (at 37°C) was 10 min (lanes 1 and 8), 1 h (lanes 4, 6, 11 and 13), or 20 h (lanes 2, 5, 7, 9, 12 and 14). In lanes 3 and 10, a 5′-end-labeled 6-mer oligoribonucleotide (pCCCUUU) served as size control to assign cleavage at the m_{-1} site.

and 12 versus 4 and 11). Under the applied holoenzyme assay conditions (buffer B), essentially no cleavage of the LNA (T-1) and 2′-OCH_3 (T-1) substrates was seen in the absence of the protein cofactor (Figure 2C, lanes 7 and 14). Thus, the protein exerted its known effect, i.e. improvement of activity under low salt conditions, but a severe catalytic defect caused by LNA (T-1) and 2′-OCH_3 at nt −1 remained despite the presence of the protein. Interestingly, the protein switched the cleavage site for the 2′-OCH_3 (T-1) ptRNA such that cleavage occurred predominantly at the m_{-1} site and not at the m_{+1} site as in the RNA-alone reaction (Figure 2C, lanes 2 versus 5). As in the RNA-alone reaction, the *E. coli* holoenzyme cleaved the LNA (T-1) substrate with low efficiency at the c_0 and m_{+1} sites, and overexposure of gels even revealed some cleavage at the m_{-1} site (Figure 2C, lane 12). Processing inhibition by LNA and 2′-OCH_3 at −1 also led to appearance of an aberrant cleavage product in reactions catalyzed by the *E. coli* holoenzyme (marked by asterisks in Figure 2C, lanes 5 and 12). This aberrant cleavage site, attributable to a minor alternative conformation of $ptRNA^{Gly}$, was tentatively assigned (data not shown) to the anticodon arm. Indeed, cleavage of such weakly populated aberrant tRNA conformers was observed before by Kikuchi and coworkers and termed hyperprocessing (38). The underlying rearrangement of the tRNA structure apparently results from base pairing between the 3′-strand of the acceptor stem and nucleotides of the variable loop and/or the 3′-strand of the anticodon stem to form a hairpin-like structure (38–40).

In the reaction catayzed by *B. subtilis* P RNA and holoenzyme, we saw very weak cleavage at the c_0 site for 2′-OCH_3 (T-1) ptRNA and at the m_{+1} and c_0 sites for LNA (T-1) ptRNA. Examples are shown in Figure 3

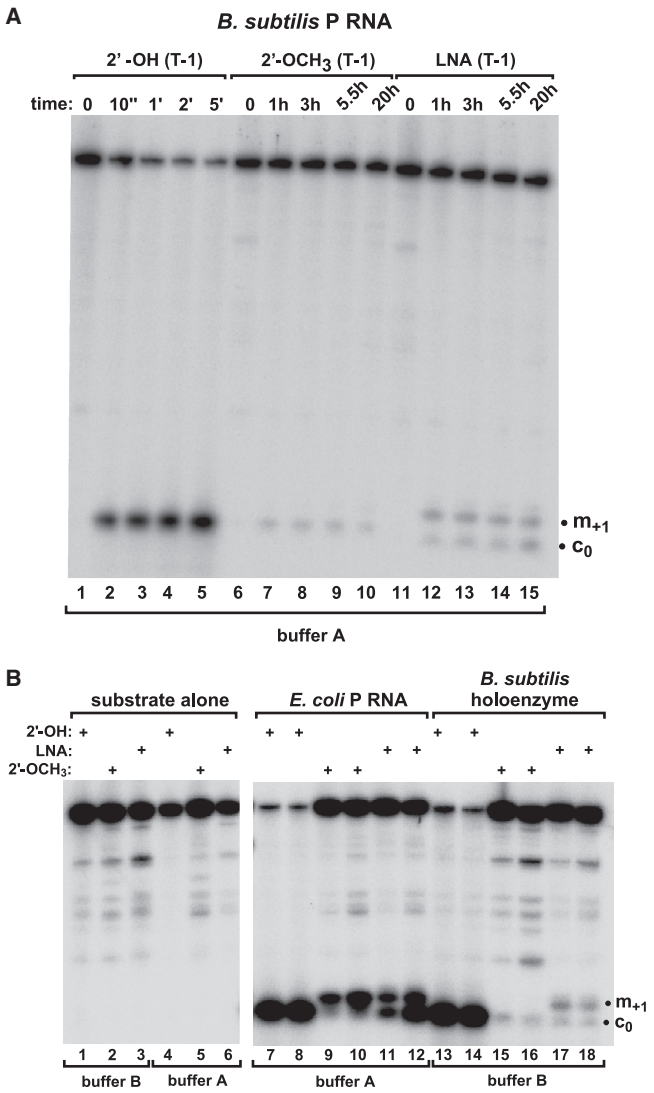

Figure 3. Processing of ptRNAs 2′-OH (T-1), 2′-OCH_3 (T-1) and LNA (T-1) by (**A**) *B. subtilis* P RNA and (**B**) the *B. subtilis* RNase P holoenzyme. (**A**) Time courses for cleavage in the presence of 5 μM *B. subtilis* P RNA, <1 nM ptRNA, 1 M NH_4OAc, 50 mM MES, pH 5.5 and 120 mM Mg^{2+}, with the two cleavage sites (c_0 and m_{+1}) indicated at the right margin. (**B**) Processing of the same three substrates by the *B. subtilis* RNase P holoenzyme (lanes 13–18) in buffer B (see legend to Figure 2); as size reference, corresponding reactions catalyzed by *E. coli* P RNA in buffer A (see legend to Figure 2) were loaded (lanes 7–12); control incubations for 20 h in the absence of enzyme were performed in buffer B (lanes 1–3) or buffer A (lanes 4–6). Incubation times were 5 min (lane 7), 20 min (lane 8), 10 min (lane 13), 30 min (lane 14), 4 h (lanes 9, 11, 15, 17) and 20 h (lanes 1–6, 10, 12, 16, 18).

for the *B. subtilis* RNA-alone reaction (Figure 3A, lanes 6–15) and the *B. subtilis* holoenzyme (Figure 3B, lanes 15–18). In conclusion, all four tested activities (*E. coli* and *B. subtilis* P RNAs and holoenzymes) cleaved the LNA (T-1) substrate with very low efficiency relative to unmodified ptRNA, and utilized the aberrant m_{+1} site in addition to the c_0 site. However, the 2′-OCH_3 (T-1) ptRNA was cleaved with very low effciency at the c_0 site by *B. subtilis* P RNA and holoenzyme, whereas *E. coli* P RNA selected exclusively the m_{+1} site and the *E. coli* holoenzyme cleaved predominantly at m_{-1} and weakly at m_{+1}.

Rate constants of cleavage by *E. coli* P RNA

All modifications introduced at nt −1 significantly affected the cleavage reaction catalyzed by *E. coli* P RNA. The rate constants for c_0 cleavage under single turnover conditions (E >> S) and rate-limiting chemistry (120 mM Mg^{2+}, pH 5.5) decreased in the order 2′-OH (T-1) ~ LNA (T-2) ~ 2′-OH (C-1) > 2′-F (C-1) > 2′-H (C-1) >> LNA (T-1), and for the 2′-OCH_3 (T-1) ptRNA no cleavage at all was detected at the c_0 site (Table 3). The same hierarchy was seen at 20 mM Mg^{2+}, pH 5.5, but at this lower Mg^{2+} concentration cleavage of the LNA (T-1) and 2′-OCH_3 (T-1) substrates was at the detection limit and thus not further analyzed. Rate differences were mitigated at pH 7 and 120 mM Mg^{2+}, which was expected because at this higher pH value cleavage rates are generally faster, but another step than cleavage chemistry begins to limit the turnover of ptRNA substrates with 2′-OH at nt −1 (20). At lower Mg^{2+} concentrations (20 mM), the defects owing to ribose modifications at nt −1 were exacerbated, consistent with the documented Mg^{2+} binding defect caused by the absence of the 2′-hydroxyl group at this location (8,20). Low efficiency cleavage of ptRNA 2′-OCH_3 (T-1) at the m_{+1} site was comparable at 20 and 120 mM Mg^{2+} (pH 7), although the endpoint of the reaction was lower at 20 mM Mg^{2+} (0.3 versus 0.55, Table 3).

Rate constants of cleavage by *B. subtilis* P RNA

In single turnover reactions (5 μM P RNA) at 120 mM Mg^{2+} and rate-limiting chemistry (pH 5.5) (10), the hierarchy of effects caused by the different ribose modifications equaled that observed for *E. coli* P RNA (cf. Tables 3 and 4), but the decreases in rate constant were more pronounced for the 2′-F (C-1) and particularly the 2′-H (C-1) ptRNA analyzed under the same conditions. Furthermore, the endpoint for c_0 cleavage of the LNA (T-1) substrate by *B. subtilis* P RNA was ~2.5% (Table 4), compared with 65% (fitted endpoint) and 42% (highest substrate conversion measured experimentally; Table 3) for the *E. coli* P RNA reaction. Another peculiarity was seen for *B. subtilis* P RNA-catalyzed cleavage of 2′-OCH_3 (T−1) ptRNA at the c_0 site and LNA (T-1) ptRNA at the m_{+1}-site. Here, cleavage was already at saturation at the first time point (1 h; Table 4 and Figure 3A, lanes 6–15), with very low endpoints (1–4%; Table 4). A possible explanation is that weakly populated E–S conformers gave rise to these cleavages.

Rate constants of cleavage by RNase P holoenzymes

Rates in the RNase P holoenzyme reactions were measured under single turnover conditions at pH 6.0 and 4 mM Mg^{2+}, or at 10 mM Mg^{2+} for the most inhibitory LNA and 2′-OCH_3 modifications. Effects were similar in reactions catalyzed by the *E. coli* and *B. subtilis* holoenzymes, with two major exceptions: (i) similar to the *B. subtilis* RNA-alone reaction, the defect caused by the 2′-H (C-1) ptRNA was much higher in the *B. subtilis*

Table 3. Observed (k_{obs}) and relative (k_{rel}) rate constants for cleavage of modified ptRNAs by *E. coli* P RNA

ptRNA	*E. coli* P RNA							
	pH 5.5				pH 7			
	20 mM Mg^{2+}		120 mM Mg^{2+}		20 mM Mg^{2+}		120 mM Mg^{2+}	
	k_{obs} (min^{-1})	k_{rel}	k_{obs} (min^{-1})	k_{rel}	k_{obs} (min^{-1})	k_{rel}	k_{obs} (min^{-1})	k_{rel}
2′-OH (T-1)	0.9 ± 0.25	1.0	3.2 ± 1.1	1.0	8.7 ± 3.9	1.0	14.5 ± 6.5	1.0
LNA (T-1) c_0 site	n.a.	n.a.	$(1 \pm 0.5) \times 10^{-3}$ $L = 0.65/0.42$	3200	$(8 \pm 5) \times 10^{-4}$ $L = 0.43/0.27$	10 875	0.024 ± 0.004 $L = 0.73/0.76$	604
LNA (T-1) m_{+1} site	n.a.	n.a.	$(2.8 \pm 0.1) \times 10^{-3}$ $L = 0.1/0.1$	1143	$(3.1 \pm 0.1) \times 10^{-3}$ $L = 0.15/0.15$	2806	$(2.2 \pm 0.1) \times 10^{-2}$ $L = 0.13/0.15$	659
2′-OCH_3 (T-1) c_0 site	n.a.	n.a.	n.d.	∞	n.d.	∞	n.d.	∞
2′-OCH_3 (T-1) m_{+1} site	n.a.	n.a.	0.0018 $L = 0.17/0.16$	1778	$(2.9 \pm 1) \times 10^{-3}$ $L = 0.3/0.3$	3000	$(3.1 \pm 1) \times 10^{-3}$ $L = 0.55/0.55$	4677
LNA (T-2)	0.52 ± 0.02[a]	1.7	2.34 ± 0.16[b]	1.4	n.a.	n.a.	n.a.	n.a.
2′-OH (C-1)	1.2 ± 0.1	0.8	5.2 ± 0.7	0.6	8.3 ± 0.5[c]	1.0	12.0 ± 2.0[b,c]	1.2
2′-F (C-1)	$(2.3 \pm 0.9) \times 10^{-2}$	39	0.5 ± 0.07	6.4	1.3 ± 0.08	6.7	7.0 ± 2.5	2.1
2′-H (C-1)	$(7 \pm 3) \times 10^{-4}$	1286	$(4.0 \pm 0.7) \times 10^{-2}$	80	$(2.8 \pm 0.6) \times 10^{-2}$	311	0.6 ± 0.15	24

n.a.: not analyzed; n.d.: cleavage not detectable. Cleavage experiments were performed under single turnover conditions (5 μM *E. coli* P RNA, <1 nM ptRNA, 1 M NH_4OAc and the indicated pH and Mg^{2+} concentration, essentially as described (30); for low efficiency cleavage of the LNA (T-1) and 2′-OCH_3 (T-1) substrates, average values for the endpoint (L = limit) of the reaction determined by curve fitting and average values for the highest substrate turnover measured experimentally are given; k_{rel} is the ratio of the respective k_{obs} value to that of the 2′-OH (T-1) ptRNA. For the LNA (T-1) and 2′-OCH_3 (T-1) substrates, cleavage is differentiated for the c_0 and m_{+1} sites; all other substrates were cleaved exclusively at the c_0 site.
[a]Ten instead of 20 mM Mg^{2+}.
[b]One hundred instead of 120 mM Mg^{2+}.
[c]Taken from ref. (20).

Table 4. Observed (k_{obs}) and relative (k_{rel}) rate constants for cleavage of modified ptRNAs by *B. subtilis* P RNA and *E. coli* and *B. subtilis* RNase P holoenzymes

ptRNA	*E. coli* holoenzyme		*B. subtilis* P RNA		*B. subtilis* holoenzyme	
	pH 6		pH 5.5		pH 6	
	4 or 10 mM Mg^{2+}		120 mM Mg^{2+}		4 or 10 mM Mg^{2+}	
	k_{obs} (min^{-1})	k_{rel}	k_{obs} (min^{-1})	k_{rel}	k_{obs} (min^{-1})	k_{rel}
2′-OH (T-1)	2.5 ± 0.5	1.0	2.64 ± 0.4	1.0	0.73 ± 0.07	1.0
LNA (T-1) c_0 site	Extent: 0.03 at 1 h; ≤0.2 at 20 h[a]		$(3 \pm 1) \times 10^{-3}$ $L = 0.027/0.027$	880	Extent: 0.03 at 1 h; 0.05 at 20 h[a]	
LNA (T-1) m_{+1} site	Extent: 0.03 at 1 h; ≤0.07 at 20 h[a]		Extent: 0.03 at 1 h; 0.04 at 20 h		Extent: 0.04 at 1 h; 0.05 at 20 h[a]	
2′-OCH_3 (T-1) c_0 site	n.d.		Extent: 0.01 at 1 and 20 h		Extent: 0.01 at 1 h; 0.02 at 23 h[a]	
2′-OCH_3 (T-1) m_{-1} site	$(6.0 \pm 0.1) \times 10^{-3}$ $L = 0.31/0.31$[a]	417	n.d.		n.d.	
2′-OH (C-1)	2.5 ± 0.2	1.0	5.8 ± 0.1	0.5	1.57 ± 0.04	0.5
2′-F (C-1)	0.39 ± 0.06	6.4	$(6.6 \pm 0.5) \times 10^{-2}$	40	0.11 ± 0.02	6.6
2′-H (C-1)	$(7.5 \pm 1.5) \times 10^{-2}$ $L = 0.19/0.17$	33	0.001 ($L = -/0.12$)[b]	2640	$(1 \pm 0.2) \times 10^{-3}$ ($L = -/0.08$)[b]	1570

n.d.: Cleavage not detectable. Cleavage experiments were performed under the following conditions: 5 μM *B. subtilis* P RNA, <1 nM ptRNA, 1 M NH_4OAc, 50 mM MES, pH 5.5 and Mg^{2+} as specified above each column or 100 nM holoenzyme, <1 nM ptRNA, 100 mM KCl, 50 mM MES, pH 6 and 4 or 10 mM Mg^{2+} (*E. coli*/*B. subtilis* holoenzyme). Holoenzyme reconstitution and kinetic experiments were performed as described under Materials and Methods. Cleavage is differentiated for the c_0 and m_{-1} site in the case of the 2′-OCH_3 (T-1) substrate, and for the c_0 and m_{+1} site in the case of ptRNA LNA (T-1); all other substrates were cleaved exclusively at the c_0 site. For the 2′-OCH_3 (T-1) and LNA (T-1) substrates, cleavage occurred to very low extents [in most cases with saturation already reached at the first data point (1 h)]; thus, only the extent of cleavage instead of cleavage rate constants is given here.
[a]Determined at 10 mM Mg^{2+}.
[b]Determined from the linear range of substrate turnover (no endpoint from curve fitting/ highest turnover experimentally measured).

than *E. coli* holoenzyme reaction; (ii) weak cleavage of the 2′-OCH_3 substrate at the c_0 site occurred with *B. subtilis* but not with *E. coli* RNase P, as mentioned before. As observed for *B. subtilis* P RNA (see above), the extent of cleavage for the LNA (T-1) and 2′-OCH_3 (T-1) substrates by both holoenzymes was extremely low (Table 4).

Mg^{2+} dependence of LNA (T-1) ptRNA cleavage by *E. coli* P RNA at sites c_0 and m_{+1}

The LNA (T-1) ptRNA was simultaneously processed at the c_0 and m_{+1} site by *E. coli* P RNA (Figure 2B and C). Simultaneous processing at different sites can be attributed to parallel reaction pathways (14,19,22,23,41) as illustrated in Scheme 1. Here we investigated the Mg^{2+} dependence of c_0 and m_{+1} cleavage, with the following outcome: First, at low [Mg^{2+}], the fraction of substrate cleaved at the c_0 site (F_c) was substantially lower at early versus late time points (Figure 4A); with increasing [Mg^{2+}], these differences largely disappeared (Figure 4B–D). This indicates that the two (E•S) complexes reacted with different single exponential decay rate constants (k_{obs}) at low [Mg^{2+}] and similar rate constants at high [Mg^{2+}]. Second, F_c values at experimental endpoints (last measured time point) and theoretical endpoints (derived from the single exponential decay curve fit) were lower at 20 mM Mg^{2+} ($F_c < 0.7$) than at e.g. 120 mM Mg^{2+} ($F_c > 0.8$). Third, plotting k_{obs} as a function of [Mg^{2+}] (Figure 4E) and allowing for a cooperative Mg^{2+} dependence at both cleavage sites (see Materials and methods section) revealed a higher Mg^{2+} dependence for cleavage at the c_0 site ($K_{1/2}$ = 184 mM) than at the aberrant m_{+1} site ($K_{1/2}$ = 129 mM), consistent with a severe metal ion binding defect for c_0 cleavage in the presence of LNA at nt −1 (the defect may include contributions from K_{conf} or k_{c_0}; see Scheme 1). A double logarithmic plot of the same data illustrates that the k_{obs} for c_0 cleavage was slower than that for m_{+1} cleavage at low [Mg^{2+}], whereas this relation was reversed at high [Mg^{2+}] (Figure 4F).

pH dependence of c_0 and m_{+1} cleavage pathways

In the hydrolysis reaction catalyzed by RNase P, a linear relationship of log k_{obs} and pH with a slope of ∼1 is taken as evidence for the catalytic step being rate-limiting (8,9,11,20,22,42). This pH dependence, consistent with a single ionization, is thought to reflect ionization of a metal ion-coordinated water molecule acting as the nucleophile in this phosphodiester hydrolysis reaction (8,11,22). Analysis of the pH dependence of log k_{obs} for cleavage of the LNA (T-1) ptRNA at sites c_0 and m_{+1} (Figure 5) revealed a slope of ∼0.9 up to pH 7 for c_0 cleavage, after which the curve inflected (Figure 5D), consistent with another step limiting the rate of the reaction above pH 7 (9). In contrast, cleavage at the m_{+1} site was linear over the entire pH range (5.5–8.1) but with a slope of only 0.45 (Figure 5D), indicative of another step than cleavage chemistry limiting the reaction at all tested pH values.

The pH variation experiments were performed at an intermediate Mg^{2+} concentration (60 mM). Interestingly, lowering the pH caused similar effects as lowering the Mg^{2+} concentration at neutral pH (Figure 4): at low pH, m_{+1} cleavage was faster than c_0 cleavage, while this relation was inversed above pH 7 (Figure 5D); and, related to this, at low versus higher pH (Figure 5A–C) the fraction of substrate cleaved at the c_0 site (F_c) was substantially lower at early than late time points.

DISCUSSION

LNA and 2′-OCH_3 modifications at nt −1: blockage of steps after substrate ground state binding

A 2′-OCH_3 modification at position −1 was previously reported as the most inhibitory substrate ribose modification in the reaction catalyzed by *E. coli* P RNA (8). In this previous study, a ptRNA with a single nucleotide as 5′-leader was miscleaved at the m_{+1} site as observed here. The substrate with a 1-nt 5′-leader precluded analysis of m_{-1} cleavage, but as shown here this site appears to be blocked by 2′-OCH_3 at nt −1 in *E. coli* P RNA-alone reactions with ptRNAs carrying longer 5′-leaders (Figure 2). The inhibitory strength of 2′-OCH_3 at −1 exceeded that of a 2′-deoxy modification, consistent with a steric effect caused by the extra methyl group (8).

Our results obtained with *E. coli* P RNA demonstrate that the transition state for canonical cleavage can be achieved in the presence of a fixed C3′-*endo* conformation at nt −1 (Figure 2B and C), indicating that a C2′-*endo* conformation prevailing at this position based on NMR analyses (26) is not an absolute requirement for catalysis to occur. It is unclear if the low efficiency of c_0 cleavage with LNA at −1 is primarily due to the steric effect of the extra methylene group or includes substantial contributions from the lack of ribose flexibility at this position. Also, the strong inhibitory effect of LNA might stem from the fact that the free electron pairs of the 2′-oxygen in LNA are orientationally constrained; this may impair the correct positioning of the Mg_B-hydrate complex containing the water molecule which we propose to protonate the 3′-oxyanion leaving group (Figure 6A). The moderate effect of LNA at −1 on substrate ground state binding (Table 2) relative to 2′-OCH_3 suggests that the extra methylene group causes less steric constraints than the 2′-OCH_3 group; likewise, the LNA (T-1) substrate was cleaved by *E. coli* P RNA at the c_0 site, whereas c_0 cleavage was not seen at all in the presence of the 2′-OCH_3 (T-1) modification (Figure 2). However, in contrast to the mild defect in substrate ground state binding, the high Mg^{2+} requirement for c_0 cleavage of LNA (T-1) ptRNA at saturating enzyme concentrations (Figure 4E) is consistent with a severe block in the binding of catalytically relevant Mg^{2+}. Thus, the defect is on K_{conf} and/or k_{c_0} rather than on K_{c_0} (Scheme 1). It should also be noted that the effect of 2′-OCH_3 at −1 on ground state binding (30-fold at 15 mM Ca^{2+}; Table 2) was still moderate compared with the complete blockage of cleavage at site c_0 for this modification. Thus, we favor a model according to which the extra methylene or methyl group causes a steric interference with the nearby bound catalytic Mg^{2+} during its re-coordination on the way to the transition state for

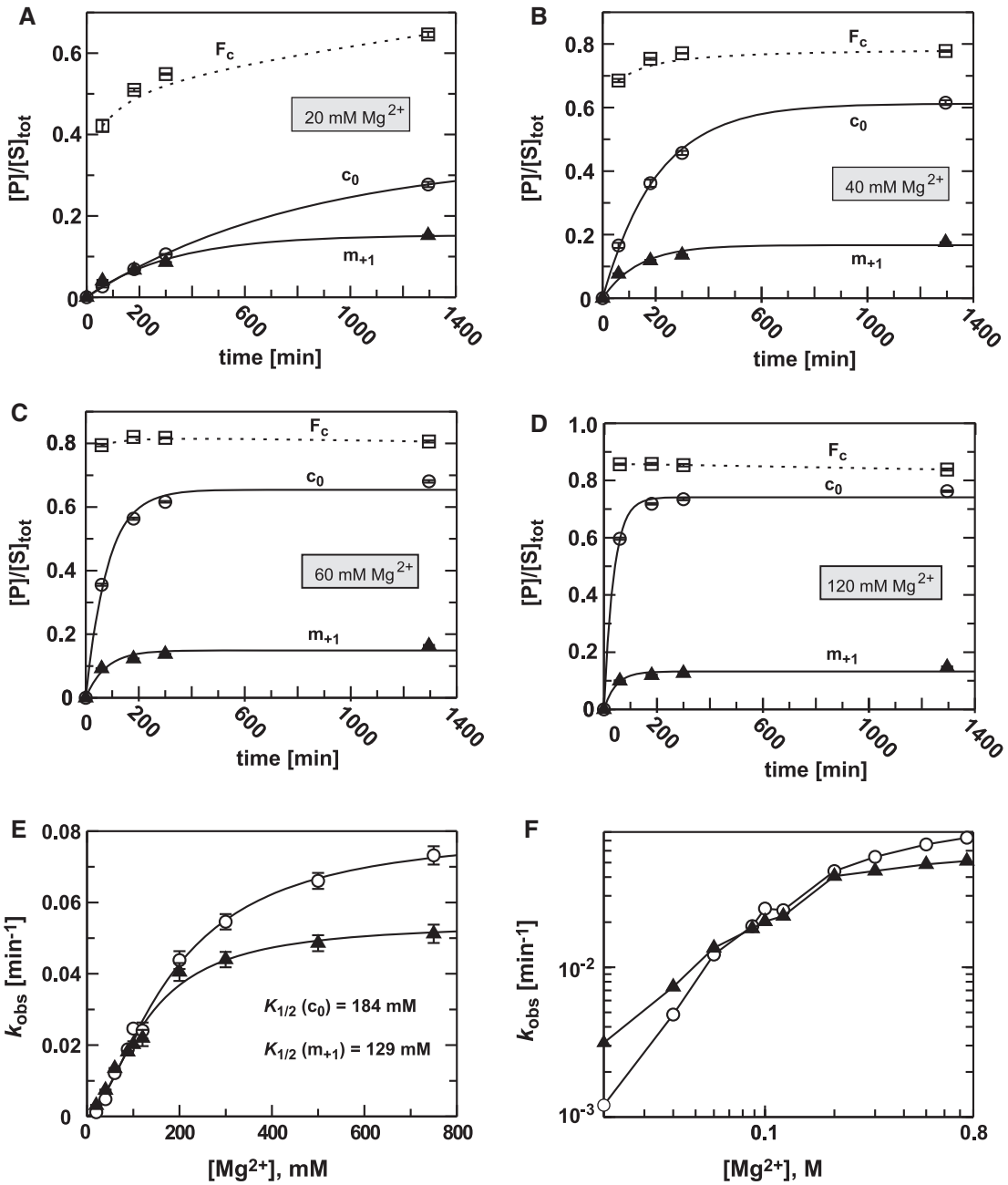

Figure 4. Processing of the LNA (T-1) substrate by *E. coli* P RNA at different Mg^{2+} concentrations. (**A–D**) Kinetic analyses of the two parallel cleavage pathways leading to cleavage at site c_0 or m_{+1}. Cleavage experiments were performed under single turnover conditions (5 μM P RNA, <1 nM ptRNA) in the presence of 1 M NH_4OAc, 50 mM PIPES, pH 7 and 60 mM Mg^{2+}. Plots representing selected Mg^{2+} concentrations show cleavage at the canonical c_0 site (open circles) and site m_{+1} (filled triangles). The fraction of substrate reacted is expressed as the ratio of product at a given time [*P*] to the total amount of substrate $[S]_{tot}$ at the start of the reaction. The relative amount of cleavage taking place at the canonical site (F_c; open squares) was calculated as the amount of c_0 product divided by the sum of c_0 and m_{+1} cleavage products. (**E**) Observed rate constants for cleavage at sites c_0 and m_{+1} as a function of Mg^{2+} concentration. Data were fitted to the Hill equation: $k_{obs} = (V_{max} \bullet [Mg^{2+}]^n)/(K' + [Mg^{2+}]^n)$, resulting in reasonable fits with $V_{max} = 0.08 \pm 0.003$, $K' = 0.066 \pm 0.02$ and $n = 1.61 \pm 0.12$ for c_0 cleavage, and $V_{max} = 0.054 \pm 0.003$, $K' = 0.03 \pm 0.017$ and $n = 1.71 \pm 0.21$ for m_{+1} cleavage; $K_{1/2}$ values were calculated as $K_{1/2} = \sqrt[n]{K'} = 184$ mM for c_0 and 129 mM for m_{+1} cleavage. (**F**) Double logarithmic presentation of the data shown in panel E to illustrate that cleavage at site c_0 was slower at low Mg^{2+} concentrations but faster at high Mg^{2+} concentrations relative to m_{+1} cleavage.

cleavage (Figure 6). To which extent the defect is exerted at the level of K_{conf} or bond breakage (k_{c_0}) cannot be discerned on the basis of our data.

Despite their similar chemical nature, the effects of LNA and 2′-OCH_3 substitutions at nt −1 differed in detail. Relevant towards understanding these differences could be the fact that the 2′-*O*-methylene group in LNA occupies a position in space that coincides only with one of the many positions that can be adopted by the 2′-OCH_3 group. The latter can rotate around the C2′-O2′ bond, and

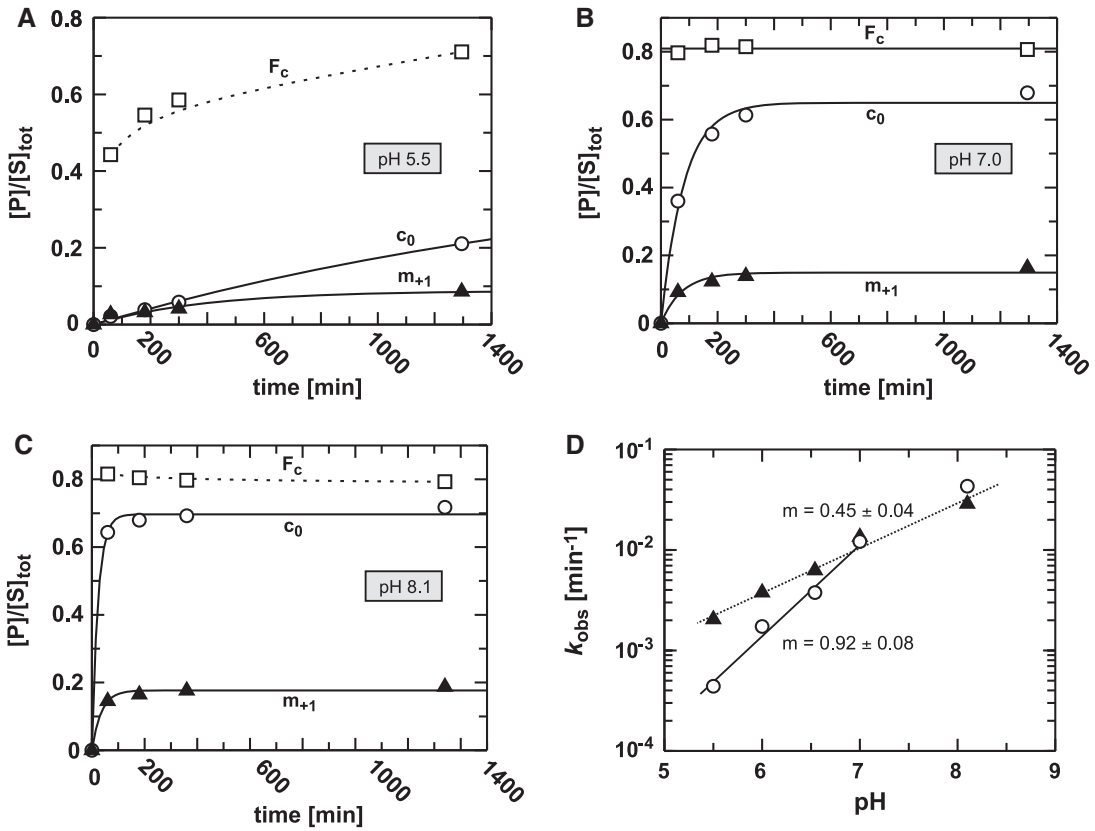

Figure 5. Kinetics of ptRNA LNA (T-1) processing by *E. coli* P RNA at different pH values. Cleavage experiments were performed under single turnover conditions (5 μM P RNA, <1 nM ptRNA) in the presence of 1 M NH_4OAc, 50 mM MES, PIPES or HEPES buffer and 60 mM Mg^{2+}. (**A–C**) Examples of kinetic analyses at low, intermediate and the highest pH tested. For further details, see legend to Figure 4. (**D**) Plots of $\log k_{obs}$ dependence on pH. For cleavage at the c_0 site (open circles), the first four data points gave a linear fit with a slope of 0.92 ± 0.08; for cleavage at the m_{+1} site (filled triangles), all five data points fit to a line with a slope of 0.45 ± 0.04.

additional orientations result from the equilibrium between C3′- and C2′-*endo* sugar puckers (Figure 7). The orientation flexibility of the 2′-OCH_3 group relative to the methylene group in LNA may explain the differential effects of the two substitutions on substrate ground state binding (Table 2). In addition, we recently showed that LNA at −1 stabilizes base pairing between T-1 and U73 (see Figure 1) (43). Thus, in the ground state the LNA (T-1) substrate is expected to adopt an extended acceptor stem structure to a larger degree than the 2′-OCH_3 (T-1) substrate. However, based on our recent results, the breaking of an additional base pair at the end of the acceptor stem leaves the energetic barrier for reaching the transition state of the chemical step for cleavage at the canonical (c_0) phosphodiester essentially unaffected (43). An effect on the aberrant m_{+1} and m_{-1} cleavage pathways cannot be excluded.

Regarding metal-dependent substrate ground state binding to *E. coli* P RNA, 2′-H and 2′-OCH_3 substituents at nt −1 were most deleterious, whereas LNA and 2′-F at this position had, overall, mild effects. We infer (i) that the absence of an H-bond donor function at the 2′-position of nt −1, as with LNA, is not crucial for substrate ground state binding; (ii) an extra 2′-methyl(ene) group has a mild effect if its position is constrained as in LNA; (iii) the mild effect of 2′-F can be explained in several ways; we favor the idea that the electronegative 2′-fluorine, as 2′-OH or LNA but in contrast to 2′-H, can accept a hydrogen bond from a metal ion-coordinated water molecule (20); this should also be the case for 2′-OCH_3, but here steric interference seems to dominate; (iv) a locked C3′-*endo* sugar pucker at nt −1 is compatible with high affinity ground state binding, indicating that the sugar pucker at this position has not to be constrained in C2′-*endo* for ground state binding, a possibility that arose from our previous NMR study (26). The observed effects were similar for *B. subtilis* P RNA, but apart from its lower substrate affinity, this RNA was less sensitive to the 2′-deoxy substitution at nt −1 (Table 2). However, sensitivity to the 2′-deoxy modification emerged in the *B. subtilis* holoenzyme reaction, where the effect of 2′-H even exceeded that of 2′-OCH_3. Possibly, the 2′-deoxy effect was masked in the *B. subtilis* P RNA-alone context owing to the generally low substrate affinity of this RNA in the absence of the protein cofactor. In summary, our results are consistent with the idea that acceptance of a hydrogen bond from a metal ion-coordinated water molecule is a key feature of the 2′-substitutent at nt −1 during substrate ground state binding.

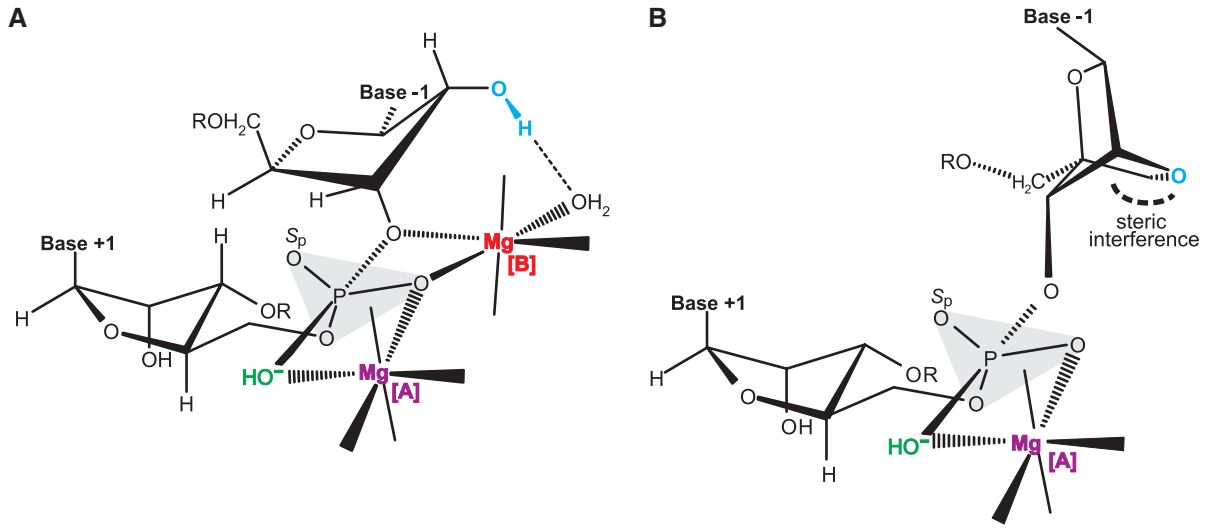

Figure 6. Transition state models for *E. coli* RNase P RNA-catalyzed phosphodiester hydrolysis at the canonical c_0 site with a ribose (**A**) or LNA (**B**) at nt −1. The model in (A) [adapted from ref. (55)] predicts that both Mg_A and Mg_B directly coordinate to the *pro-R*p oxygen, with Mg_A coordinating the OH^- nucleophile, and Mg_B interacting with the 3′-oxygen and the 2′-hydroxyl group at nt −1 via a water molecule of its hydration shell; we propose this water molecule to donate the proton to the 3′-oxyanion leaving group. The ribose at nt −1 is assumed to mainly populate the 2′-*endo* sugar pucker based on NMR analyses of acceptor stem mimics (26). (**B**) Here, the −1 nucleotide is LNA with the sugar moiety fixed in the C3′-*endo* conformation; the steric interference caused by LNA or 2′-OCH_3 at position −1 (indicated by the dashed curved line) likely disrupts the binding site for Mg_B. The model differs from others [e.g. (56)] by assuming that only two instead of three metal ions are essential; also, in our model Mg_B is proposed to simultaneously interact with the *pro-R*p oxygen, the 3′-oxygen and the 2′-OH, whereas the latter interaction is assigned to the third metal ion in the model by Kazantsev and Pace (56). Group I intron ribozymes have a similar size as bacterial P RNA and also catalyze phosphoryl transfer reactions yielding products with 3′-OH termini. The two-metal-ion mechanistic model we propose here is essentially identical to that for the second step of group I intron splicing inferred from a crystal structure of the *Azoarcus sp.* $ptRNA^{Ile}$ group I intron (57), with two differences: (i) the contact of Mg_B to the 2′-OH is outer-sphere in the RNase P reaction, but inner-sphere in the group I intron reaction; (ii) the nucleophile is a hydroxide in the RNase P reaction, but the terminal 3′-OH of the 5′-exon in the second step of the group I intron reaction (57). Despite striking similarities, one mechanistic difference has been observed in phosphodiester hydrolysis reactions catalyzed by the *Tetrahymena* group I intron-derived ribozyme and *E. coli* P RNA: whereas a 2′-amino modification at ptRNA position −1 inhibited cleavage at the canonical site with increasing protonation of the 2′-amine in the P RNA reaction (consistent with electrostatic repulsion of a metal ion), the reverse was seen with the *Tetrahymena* ribozyme; in the latter reaction, protonation of the 2′-amine at equivalent position rather stimulated cleavage at the canonical site (20,58). The molecular basis of this difference is not clear at present.

Cleavage fidelity

For simple class I tRNAs, such as the $ptRNA^{Gly}$ used here or *B. subtilis* $ptRNA^{Asp}$ (22), it has previously been discussed that interactions between *E. coli* P RNA and the ptRNA cleavage site are of redundant nature. For example, base identity switches at nt −1 that weaken the interaction with A248 of *E. coli* P RNA, 2′-substitutions at nt −1 (e.g. 2′-H or 2′-F), an *R*p-phosphorothioate substitution at the scissile phosphodiester or a G292C or G293C mutation in the CCA-binding site of P RNA do not by themselves lead to substantial miscleavage (22). However pairwise modification, such as 2′-deoxy modification at nt −1 combined with an A248U or G292C mutation resulted in substantial miscleavage (20,22). In contrast, LNA and 2′-OCH_3 at nt −1 induced severe miscleavage in the absence of any other modification, emphasizing the deleterious effect of the extra methyl(ene) group on cleavage chemistry or a preceding conformational rearrangement of E•S complexes (Scheme 1).

Differences in the Mg^{2+} and pH dependence of the correct (c_0) and mis-cleavage (m_{+1}) pathways

Harris and coworkers recently demonstrated communication between a 2′-deoxy modification at nt −1 and weakening of the A248/nt −1 contact. Alterations at both sites, such as combination of 2′-deoxy U-1 $ptRNA^{Asp}$ with the A248U mutant *E. coli* P RNA, resulted in cleavage at the c_0, m_{-1} and also at the m_{+1} site (22). When studying the proportion of cleavage events at the c_0 and m_{-1} site as a function of the Mg^{2+} concentration, the authors observed increased utilization of the m_{-1} site with increasing Mg^{2+} concentration. They concluded that the pathway leading to cleavage at the c_0 site exhibits a greater apparent affinity for Mg^{2+} than the pathway leading to cleavage at the m_{-1} site (22). We performed a similar analysis for the m_{+1} site in the presence of LNA at −1 (Figure 4) and observed a reverse correlation: here the amount of cleavage at the c_0 site increased with increasing Mg^{2+}, indicating that the LNA modification lowers the apparent affinity for Mg^{2+} of the canonical cleavage pathway below that of the pathway leading to m_{+1} cleavage.

The same authors (22) observed that F_c remained essentially constant over time in *E. coli* P RNA cleavage of ptRNAs with 2′-deoxy modifications at nt −1 and/or mutations at A248 of P RNA. Thus, they assumed that cleavages at the canonical and aberrant site (m_{-1} in their case) follow the same single exponential decay rate (k_{obs}) calculated from the sum of the c_0 and m_{+1} site cleavage products accumulating at individual time points. Using F_c and k_{obs}, the apparent first-order rate constant for

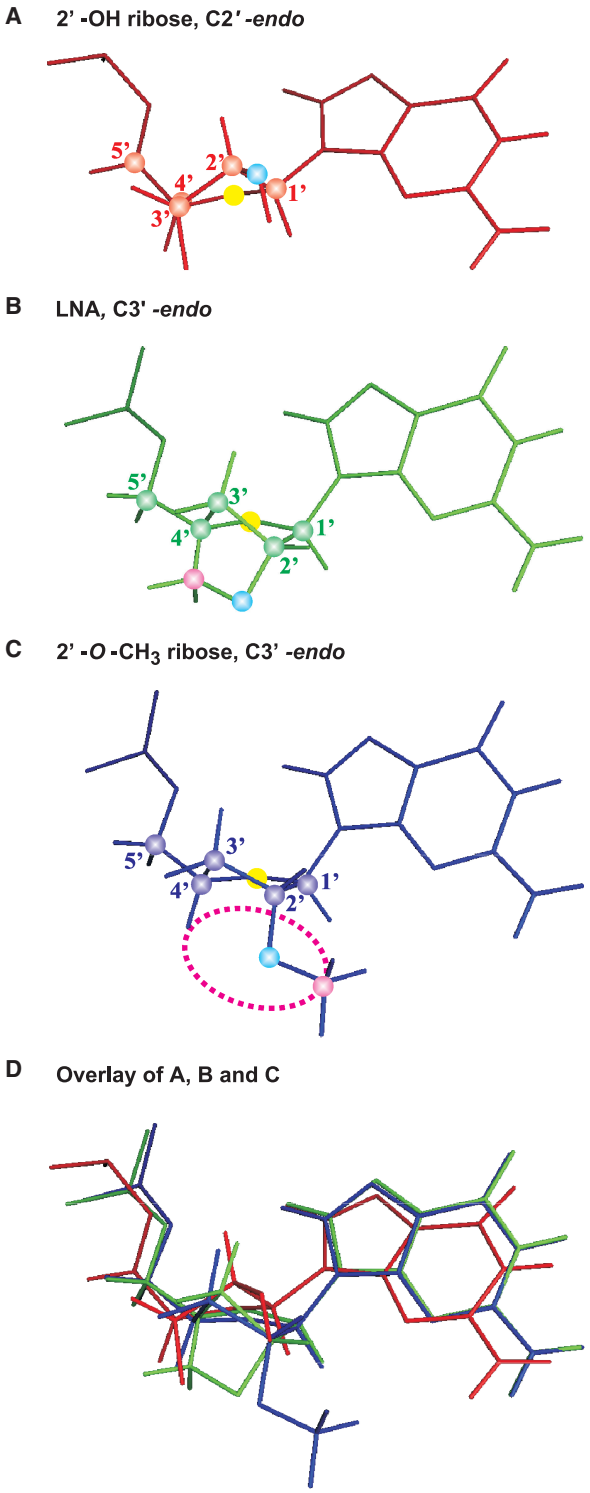

Figure 7. Illustration of commonalities and differences between 2′-OCH_3 and LNA. (**A**) Conformation of the ribose at nt −1 assuming a preference for the C2′-*endo* pucker at this position (26); (**B**) for LNA; (**C**) for 2′-OCH_3-modified ribose in the C3′-*endo* conformation; (**D**) overlay of structures shown in panel A, B and C.

cleavage (k_{app}) at a particular site was calculated according to $k_{app}[c_0] = F_c \times k_{obs}$, and $k_{app}[m_{-1}] = (1 - F_c) \times k_{obs}$ [for details, see ref. (22)]. Although this assumption also holds for our data obtained at Mg^{2+} concentrations between 60 and 200 mM (Figure 4F), it is not applicable particularly to the F_c and k_{obs} data obtained under conditions of low [Mg^{2+}] and low pH (see Figures 4A, F and 5A). Changes in F_c and $k_{obs}[c_0]$ may include contributions from the equilibria described by K_{c_0} and $K_{conf}[c_0]$ (and the corresponding forward and back rate constants) as well as k_{c_0} (see Scheme 1). Our findings (F_c increases with [Mg^{2+}], $k_{obs}[c_0] < k_{obs}[m_{+1}]$ at low [Mg^{2+}] and pH, $k_{obs}[c_0] > k_{obs}[m_{+1}]$ at high [Mg^{2+}] and high pH) can be explained within the following framework (also illustrated in Scheme 2): When enzyme and substrate are mixed, rapid equilibria of $(E\bullet S)c_0$ and $(E\bullet S)m_{+1}$ form, which commit the complexes to reaction along the different pathways. Partitioning between $(E\bullet S)c_0$ and $(E\bullet S)m_{+1}$ is sensitive to the Mg^{2+} concentration. At low [Mg^{2+}], the ratio of equilibrium binding constants $K_{c_0}/K_{m_{+1}}$ (Scheme 1) exceeds that at higher [Mg^{2+}], explaining why F_c increased with [Mg^{2+}] (Figure 4A–D). The rate constant for bond breakage at the c_0 site (k_{c_0}) and/or the preceding conformational step ($K_{conf}[c_0]$; see Scheme 1) have a higher Mg^{2+} requirement than that for m_{+1} cleavage (Figure 4F). Finally, different steps are rate-limiting for cleavage at sites c_0 and m_{+1}, as inferred from the different pH dependencies between pH 5.5 and 7.0 (Figure 5D).

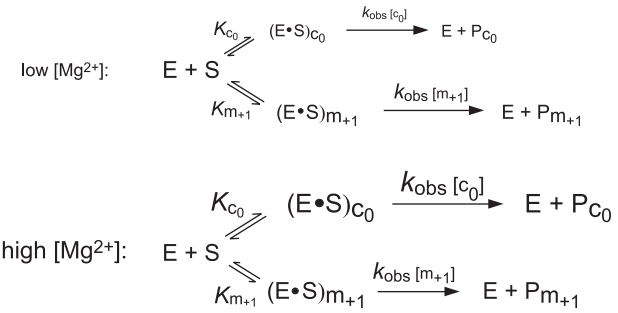

Scheme 2. Illustration of the differential effects of Mg^{2+} concentration on the parallel pathways for cleavage of the LNA (T-1) substrate by *E. coli* P RNA, using a simplified version of Scheme 1. At low [Mg^{2+}], the proportion of $(E\bullet S)c_0$ complexes is lower than at high [Mg^{2+}] (indicated by differences in letter size); also, increasing [Mg^{2+}] increases the observed rate constant for cleavage at the c_0 site, $k_{obs}[c_0]$, more than $k_{obs}[m_{+1}]$; changes in k_{obs} may include effects on K_{conf} and/or the chemical step (k_{c_0} and $k_{m_{+1}}$, respectively; see Scheme 1).

Suppression of m_{-1} cleavage

Another idiosyncrasy of LNA or 2′-OCH_3 at −1 is the complete absence of cleavage by *E. coli* P RNA at the m_{-1} site (Figure 2B and C), which represents the prevailing miscleavage site [e.g. (44)]. Pan and colleagues showed that a 2′-deoxy substitution at −1 in ptRNA not only decreased the cleavage rate constant by *B. subtilis* P RNA 240-fold for the c_0 site but also 470-fold for the m_{-1} site and 210-fold for another aberrant site (between nt +2 and +3). This finding suggested a contact between the ribozyme and the ptRNA substrate 2′-OH at −1 which promotes a conformational rearrangement required for catalysis at both the c_0 as well as at aberrant sites, such as the m_{-1} site (19,24). Blockage of cleavage at the unmodified m_{-1} site owing to LNA or 2′-OCH_3 at −1 would be consistent with the findings of Loria and Pan

(19,24). Based on their model, utilization of the m_{+1} site in *E. coli* P RNA-catalyzed cleavage of ptRNA LNA (T-1) or 2′-OCH_3 (T-1) may suggest that the 2′-OH group at nt +1 took over the role of that at nt −1 in promoting the conformational step preceding catalysis (Scheme 1). Likewise, redirection of cleavage from the m_{+1} to the m_{-1} site in the 2′-OCH_3 (T-1) substrate when cleaved by the *E. coli* RNase P holoenzyme (Figure 2C) may be due to the protein cofactor allowing utilization of the 2′-OH at nt −2 as anchor point for the conformational step (24).

pH dependence of c_0 and m_{+1} cleavage by *E. coli* P RNA

The shallow pH dependence of $\log k_{obs}$ for cleavage at the m_{+1} site is consistent with one or more slow steps upstream of the hydrolysis step in the miscleavage pathway, such as conformational rearrangements. Our findings and those of others (22,45) indicate that cleavage at different sites (c_0, m_{-1}, m_{+1} or others) has different pH and metal ion dependencies and involves different contributions from rate-limiting steps. Accordingly, E–S complexes leading to cleavage at the different sites are structurally distinct. Cleavage at the c_0 site has usually the highest apparent metal ion affinity, which still pertains to 'mild' modifications, such as 2′-deoxy at nt −1. However, more deleterious modifications, such as LNA or 2′-OCH_3 at –1, can break this rule (Figure 4E). Considering that LNA at nt −1 had little effect on substrate binding in the ground state, this modification is a paradigm for a modification that specifically inhibits formation of later steps along the cleavage pathway.

Cleavage of modified substrates by *B. subtilis* P RNA

Loria and Pan (19) have studied processing of yeast $ptRNA^{Phe}$ by *B. subtilis* P RNA, representing a tRNA with a canonical 7-bp acceptor stem as the $ptRNA^{Gly}$ used in our investigation (Figure 1). They observed substantial miscleavage of $ptRNA^{Phe}$, particularly at the m_{-1} site and even in the absence of any ribose modifications. In contrast, we did not observe significant miscleavage by *B. subtilis* P RNA for any of the $ptRNA^{Gly}$ variants used here, except for the LNA (T-1) substrate which gave rise to cleavage at the m_{+1} site (Table 4). Even the 2′-OCH_3 (T-1) variant was cleaved exclusively at the c_0 site (Figure 3), in contrast to *E. coli* P RNA which entirely miscleaved this substrate. Thus, we observed little propensity of *B. subtilis* P RNA to miscleave the $ptRNA^{Gly}$ substrate. The discrepancy to the previously observed miscleavage of yeast $ptRNA^{Phe}$ (19) may be explained by the fact that yeast $ptRNA^{Phe}$ has a rather labile acceptor stem with 3 A–U and 1 G–U bp in a row in its lower part; in comparison, the acceptor stems of *B. subtilis* $tRNA^{Phe}$ molecules consist of 6 G–C and a single A–U bp, which is more typical of bacterial tRNAs. Low rigidity of the tRNA body is expected to cause conformational heterogeneity, which would explain increased miscleavage. This further raises the question if miscleavage at a specific site necessarily proceeds along the same mechanistic pathway for ptRNAs with rigid and less rigid tRNA bodies.

Cleavage of modified substrates by the *E. coli* RNase P holoenzyme

In several previous analyses, essentially identical miscleavage patterns were observed in *E. coli* P RNA-alone and holoenzyme reactions. This pertains, for example, to the disruption of the 3′-CCA interaction by mutation (36,46), or to reactions utilizing a A248U mutant P RNA and a ptRNA with a 2′-deoxy-U at nt −1 (41). However, in a study investigating the effect of a substrate 2′-amino modification at nt −1 on cleavage by *E. coli* RNase P (RNA), the P protein suppressed miscleavage at the m_{-1} site and redirected cleavage to the c_0 site (21). This suggests that effects of the P protein on cleavage fidelity depend on the specific structural alteration.

The cleavage site of the 2′-OCH_3 (T-1) substrate was almost entirely shifted from the m_{+1} to the m_{-1} site in the *E. coli* holoenzyme versus P RNA-alone reaction (Figure 2C, lanes 2 and 5). With LNA at −1, also some cleavage at the m_{-1} site appeared in the presence of the protein cofactor (Figure 2C, lanes 9 and 12). Evidently, the protein, by providing additional substrate binding energy and by enhancing the affinity of key metal ions, modulates the activation barriers of pathways leading to cleavage at different sites. The differences in mono- and di-valent salt conditions used in RNA-alone and holoenzyme reactions may also have contributed to the observed protein-dependent changes, resulting in differential effects on the individual miscleavage pathways. Specifically, the shift of cleavage site for the 2′-OCH_3 (T-1) substrate may be explained by $(E\bullet S)m_{-1}$ complex formation favored over that of $(E\bullet S)m_{+1}$ complexes in the context of the holoenzyme reaction, and/or by a differential effect of the protein on the individual equilibrium docking steps [$(E\bullet S) \rightarrow (E\bullet S)^*$; Scheme 1] preceding catalysis (24). The protein might also affect active site architecture more profoundly than as yet thought.

Differences between *E. coli* and *B. subtilis* RNase P (RNA)

Architectural differences between bacterial P RNAs of type A (for 'ancestral') and type B (for 'Bacillus') (33) are associated with biochemical differences. The *B. subtilis* RNase P holoenzyme binds ptRNA with a much higher affinity than mature tRNA, but this discrimination against mature tRNA is much less pronounced for *E. coli* RNase P (34,35). RNase P enzymes containing the *B. subtilis* P RNA are less prone to aberrant cleavage than those including *E. coli* P RNA (36), and *B. subtilis* P RNA alone binds ptRNA substrates weaker than its *E. coli* counterpart (37, this study). The *E. coli* protein reduces the Mg^{2+} concentration requirement for tertiary structure formation of P RNA and increases the melting temperature at physiologically relevant Mg^{2+} concentrations (37). In contrast, the *B. subtilis* protein does not exert such stabilizing effects on its cognate or *E. coli* P RNA (37). Taking these reported differences between the two RNase P model systems into account, it is not surprising that we saw differences and commonalities (for details, see Results). Differences included a stronger defect caused

by 2′-H at nt −1 on the *B. subtilis* versus *E. coli* holoenzyme, and deviating cleavage site selection for the 2′-OCH_3 substrate; major commonalities included the severe catalytic block by LNA and 2′-OCH_3 and, for the LNA substrate, the occurrence of low efficiency parallel cleavage pathways leading to hydrolysis at the c_0 and m_{+1} sites. The differences illustrate the complex interplay of functional groups and of thermodynamic as well as kinetic parameters in this RNA-catalyzed and protein-assisted phosphodiester hydrolysis reaction. Compared with protein enzyme orthologs with rigid and strongly conserved active sites, type A and B RNase P enzymes appear more as homologs that still catalyze the same reactions, but with distinct architectural and non-identical mechanistic concepts.

The P protein is unable to compensate the catalytic block by LNA

The protein subunit of bacterial RNase P increases substrate affinity and specificity (47,48), stabilizes the local RNA conformation (37), preorganizes S- and C-domain orientation (24) and increases the affinity of catalytically important divalent metal ions (11). For *B. subtilis*, it has been shown that the P protein interacts with the 5′-leader of tRNA precursor thus increasing substrate affinity (37,49) while reducing the contact area to the T stem-loop region of tRNA substrates relative to P RNA alone (50). Recently, the binding affinity and processing efficiency of a set of *E. coli* ptRNA substrates with different 5′-leaders and bodies was investigated in the absence and presence of the protein cofactor (51). The results indicated that the protein confers the capacity to the *E. coli* RNase P holoenzyme to bind all 5′-pre-tRNAs with uniform affinity. Apparently, this capacity was achieved during evolution by combining suboptimal tRNA structures with 5′-leader sequences that confer high ptRNA affinity (51). Such a thermodynamic compensation effect was also seen here for binding of the 2′-OCH_3 (T-1) ptRNA, where defects of binding to *E. coli* and *B. subtilis* P RNA were alleviated by the presence of the protein cofactor (Table 2). In contrast, the dramatic inhibitory effect on P RNA catalysis caused by LNA and 2′-OCH_3 at nt −1 remained in the holoenzyme reaction, indicating that these modifications block E•S* formation and/or the bond breakage step itself. Finally, our results demonstrate that LNA enriches the nucleotide analog toolbox for mechanistic enzyme studies.

ACKNOWLEDGEMENTS

The authors thank Stefan Limmer and Philipp Hadwiger (Ribopharma AG, Kulmbach, Germany) for the synthesis of RNA oligonucleotides, and Dominik Helmecke for excellent technical assistance.

FUNDING

Deutsche Forschungsgemeinschaft [HA 1672/7-4/5] and the Fonds der Chemischen Industrie. Funding for open access charge: Deutsche Forschungsgemeinschaft (HA 1672/7-4/5).

Conflict of interest statement. None declared.

REFERENCES

1. Schön,A. (1999) Ribonuclease P: the diversity of a ubiquitous RNA processing enzyme. *FEMS Microbiol. Rev.*, **23**, 391–406.
2. Hartmann,E. and Hartmann,R.K. (2003) The enigma of ribonuclease P evolution. *Trends Genet.*, **19**, 561–569.
3. Walker,S.C. and Engelke,D.R. (2006) Ribonuclease P: the evolution of an ancient RNA enzyme. *Crit. Rev. Biochem. Mol. Biol.*, **41**, 77–102.
4. Evans,D., Marquez,S.M. and Pace,N.R. (2006) RNase P: interface of the RNA and protein worlds. *Trends Biochem. Sci.*, **31**, 333–341.
5. Holzmann,J., Frank,P., Loffler,E., Bennett,K.L., Gerner,C. and Rossmanith,W. (2008) RNase P without RNA: identification and functional reconstitution of the human mitochondrial tRNA processing enzyme. *Cell*, **135**, 462–474.
6. Guerrier-Takada,C., Gardiner,K., Marsh,T., Pace,N. and Altman,S. (1983) The RNA moiety of ribonuclease P is the catalytic subunit of the enzyme. *Cell*, **35**, 849–857.
7. Brown,J.W. (1999) The Ribonuclease P Database. *Nucleic Acids Res.*, **27**, 314.
8. Smith,D. and Pace,N.R. (1993) Multiple magnesium ions in the ribonuclease P reaction mechanism. *Biochemistry*, **32**, 5273–5281.
9. Warnecke,J.M., Fürste,J.P., Hardt,W.-D., Erdmann,V.A. and Hartmann,R.K. (1996) Ribonuclease P (RNase P) RNA is converted to a Cd^{2+}-ribozyme by a single Rp-phosphorothioate modification in the precursor tRNA at the RNase P cleavage site. *Proc. Natl Acad. Sci. USA*, **93**, 8924–8928.
10. Warnecke,J.M., Held,R., Busch,S. and Hartmann,R.K. (1999) Role of metal ions in the hydrolysis reaction catalyzed by RNase P RNA from *Bacillus subtilis*. *J. Mol. Biol.*, **290**, 433–445.
11. Kurz,J.C. and Fierke,C.A. (2002) The affinity of magnesium binding sites in the *Bacillus subtilis* RNase P • pre-tRNA complex is enhanced by the protein subunit. *Biochemistry*, **41**, 9545–9558.
12. Kufel,J. and Kirsebom,L.A. (1998) The P15-loop of *Escherichia coli* RNase P RNA is an autonomous divalent metal ion binding domain. *RNA*, **4**, 777–788.
13. Brännvall,M. and Kirsebom,L.A. (2001) Metal ion cooperativity in ribozyme cleavage of RNA. *Proc. Natl Acad. Sci. USA*, **98**, 12943–12947.
14. Brännvall,M., Pettersson,F. and Kirsebom,L.A. (2002) The residue upstream of the RNase P cleavage site is a positive determinant. *Biochimie*, **84**, 693–703.
15. Christian,E.L., Kaye,N.M. and Harris,M.E. (2002) Evidence for a polynuclear metal ion binding site in the catalytic domain of ribonuclease P RNA. *EMBO J.*, **21**, 2253–2262.
16. Forster,A.C. and Altman,S. (1990) External guide sequences for an RNA enzyme. *Science*, **249**, 783–786.
17. Perreault,J.-P. and Altman,S. (1992) Important 2′-hydroxyl groups in model substrates for M1 RNA, the catalytic RNA subunit of RNase P from *Escherichia coli*. *J. Mol. Biol.*, **226**, 399–409.
18. Perreault,J.-P. and Altman,S. (1993) Pathway of activation by magnesium ions of substrates for the catalytic subunit of RNase P RNA from *Escherichia coli*. *J. Mol. Biol.*, **230**, 750–756.
19. Loria,A. and Pan,T. (1998) Recognition of the 5′ leader and the acceptor stem of a pre-tRNA substrate by the ribozyme from *Bacillus subtilis* RNase P. *Biochemistry*, **37**, 10126–10133.
20. Persson,T., Cuzic,S., Siedler,S. and Hartmann,R.K. (2003) Catalysis by RNase P RNA: unique features and unprecedented active site plasticity. *J. Biol. Chem.*, **278**, 43394–43401.
21. Brännvall,M., Kikovska,E. and Kirsebom,L.A. (2004) Cross talk between the C73/294 interaction and the cleavage site in RNase P RNA mediated cleavage. *Nucleic Acids Res.*, **32**, 5418–5429.
22. Zahler,N.H., Sun,L., Christian,E.L. and Harris,M.E. (2005) The pre-tRNA nucleotide base and 2′-hydroxyl at N(-1) contribute to fidelity in tRNA processing by RNase P. *J. Mol. Biol.*, **345**, 969–985.

23. Brännvall,M. and Kirsebom,L.A. (2005) Complexity in orchestration of chemical groups near different cleavage sites in RNase P RNA mediated cleavage. *J. Mol. Biol.*, **351**, 251–257.
24. Loria,A. and Pan,T. (1999) The cleavage step of ribonuclease P catalysis is determined by ribozyme substrate interactions both distal and proximal to the cleavage site. *Biochemistry*, **38**, 8612–8620.
25. Zuleeg,T., Hartmann,R.K., Kreutzer,R. and Limmer,S. (2001) NMR spectroscopic evidence for Mn^{2+} (Mg^{2+}) binding to a *precursor*-tRNA microhelix near the potential RNase P cleavage site. *J. Mol. Biol.*, **305**, 181–189.
26. Zuleeg,T., Hansen,A., Pfeiffer,T., Schubel,H., Kreutzer,R., Hartmann,R.K. and Limmer,S. (2001) Correlation between processing efficiency for ribonuclease P minimal substrates and conformation of the nucleotide -1 at the cleavage position. *Biochemistry*, **40**, 3363–3369.
27. Brännvall,M., Pettersson,B.M. and Kirsebom,L.A. (2003) Importance of the +73/294 interaction in *Escherichia coli* RNase P RNA substrate complexes for cleavage and metal ion coordination. *J. Mol. Biol.*, **325**, 697–709.
28. Singh,S.K., Nielsen,P., Koshkin,A.A. and Wengel,J. (1998) LNA (locked nucleic acid): synthesis and high-affinity acid recognition. *Chem. Commun.*, **4**, 455–456.
29. Petersen,M., Bondensgaard,K., Wengel,J. and Jacobsen,J.P. (2002) Locked nucleic acid (LNA): NMR solution structure of LNA:RNA hybrids. *J. Am. Chem. Soc.*, **124**, 5974–5982.
30. Cuzic,S. and Hartmann,R.K. (2007) A 2′-methyl or 2′-methylene group at G+1 in precursor tRNA interferes with Mg^{2+} binding at the enzyme-substrate interface in E-S complexes of *E. coli* RNase P. *Biol. Chem.*, **388**, 717–726.
31. Marszalkowski,M., Teune,J.H., Steger,G., Hartmann,R.K. and Willkomm,D.K. (2006) Thermostable RNase P RNAs lacking P18 identified in the *Aquificales*. *RNA*, **12**, 1915–1921.
32. Busch,S., Kirsebom,L.A., Notbohm,H. and Hartmann,R.K. (2000) Differential role of the intermolecular base-pairs G292-C_{75} and G293-C_{74} in the reaction catalyzed by *Escherichia coli* RNase P RNA. *J. Mol. Biol.*, **299**, 941–951.
33. Hall,T.A. and Brown,J.W. (2001) The ribonuclease P family. *Methods Enzymol.*, **341**, 56–77.
34. Kurz,J.C., Niranjanakumari,S. and Fierke,C.A. (1998) Protein component of *Bacillus subtilis* RNase P specifically enhances the affinity for precursor-$tRNA^{Asp}$. *Biochemistry*, **37**, 2393–2400.
35. Tallsjö,A. and Kirsebom,L.A. (1993) Product release is a rate-limiting step during cleavage by the catalytic RNA subunit of *Escherichia coli* RNase P. *Nucleic Acids Res.*, **21**, 51–57.
36. Wegscheid,B., Condon,C. and Hartmann,R.K. (2006) Type A and B RNase P RNAs are interchangeable *in vivo* despite substantial biophysical differences. *EMBO Reports*, **7**, 411–417.
37. Buck,A.H., Dalby,A.B., Poole,A.W., Kazantsev,A.V. and Pace,N.R. (2005) Protein activation of a ribozyme: the role of bacterial RNase P protein. *EMBO J.*, **24**, 3360–3368.
38. Kikuchi,Y. and Sasaki,N. (1992) Hyperprocessing of tRNA by the catalytic RNA of RNase P. Cleavage of a natural tRNA within the mature tRNA sequence and evidence for an altered conformation of the substrate tRNA. *J. Biol. Chem.*, **267**, 11972–11976.
39. Hori,Y., Sakai,E., Tanaka,T. and Kikuchi,Y. (2001) Hyperprocessing reaction of tRNA by *Bacillus subtilis* ribonuclease P ribozyme. *FEBS Lett.*, **505**, 337–339.
40. Ando,T., Tanaka,T., Hori,Y. and Kikuchi,Y. (2002) Kinetics of hyperprocessing reaction of human tyrosine tRNA by ribonuclease P ribozyme from *Escherichia coli*. *Biosci. Biotechnol. Biochem.*, **66**, 1967–1971.
41. Zahler,N.H., Christian,E.L. and Harris,M.E. (2003) Recognition of the 5′ leader of pre-tRNA substrates by the active site of ribonuclease P. *RNA*, **9**, 734–745.
42. Loria,A. and Pan,T. (1997) Recognition of the T stem-loop of a pre-tRNA substrate by the ribozyme from *Bacillus subtilis* ribonuclease P. *Biochemistry*, **36**, 6317–6325.
43. Cuzic,S., Heidemann,K.A., Wöhnert,J. and Hartmann,R.K. (2008) *Escherichia coli* RNase P RNA: substrate ribose modifications at G+1, but not nucleotide −1/+73 base pairing, affect the transition state for cleavage chemistry. *J. Mol. Biol.*, **379**, 1–8.
44. Kirsebom,L.A. (2002) RNase P RNA-mediated catalysis. *Biochem. Soc. Trans.*, **30**, 1153–1158.
45. Kufel,J. and Kirsebom,L.A. (1994) Cleavage site selection by M1 RNA, the catalytic subunit of *Escherichia coli* RNase P, is influenced by pH. *J. Mol. Biol.*, **244**, 511–521.
46. Svärd,S.G., Kagardt,U. and Kirsebom,L.A. (1996) Phylogenetic comparative mutational analysis of the base-pairing between RNase P RNA and its substrate. *RNA*, **2**, 463–472.
47. Gopalan,V., Baxevanis,A.D., Landsman,D. and Altman,S. (1997) Analysis of the functional role of conserved residues in the protein subunit of Ribonuclease P from *Escherichia coli*. *J. Mol. Biol.*, **267**, 818–829.
48. Tsai,H.Y., Masquida,B., Biswas,R., Westhof,E. and Gopalan,V. (2003) Molecular modeling of the three-dimensional structure of the bacterial RNase P holoenzyme. *J. Mol. Biol.*, **325**, 661–675.
49. Crary,S.M., Niranjanakumari,S. and Fierke,C.A. (1998) The protein component of *Bacillus subtilis* ribonuclease P increases catalytic efficiency by enhancing interactions with the 5′ leader sequence of pre-$tRNA^{Asp}$. *Biochemistry*, **37**, 9409–9416.
50. Loria,A., Niranjanakumari,S., Fierke,C.A. and Pan,T. (1998) Recognition of a pre-tRNA substrate by the *Bacillus subtilis* RNase P holoenzyme. *Biochemistry*, **37**, 15466–15473.
51. Sun,L., Campbell,F.E., Zahler,N.H. and Harris,M.E. (2006) Evidence that substrate-specific effects of C5 protein lead to uniformity in binding and catalysis by RNase P. *EMBO J.*, **25**, 3998–4007.
52. Petersen,M., Nielsen,C.B., Nielsen,K.E., Jensen,G.A., Bondensgaard,K., Singh,S.K., Rajwanshi,W.K., Koshkin,A.A., Dahl,B.M., Wengel,J. *et al.* (2000) The conformations of locked nucleic acids (LNA). *J. Mol. Recogn.*, **13**, 44–53.
53. Guschlbauer,W. and Jankowski,K. (1980) Nucleoside conformation is determined by the electronegativity of the sugar substituent. *Nucleic Acids Res.*, **8**, 1421–1433.
54. Cramer,C.J. and Truhlar,D.G. (1992) AM1-SM2 and PM3-SM3 parameterized SCF solvation models for free energies in aqueous solution. *J. Comput. Aided Mol. Des.*, **6**, 629–666.
55. Cuzic,S. and Hartmann,R.K. (2005) Studies on *Escherichia coli* RNase P RNA with Zn^{2+} as the catalytic cofactor. *Nucleic Acids Res.*, **33**, 2464–2474.
56. Kazantsev,A.V. and Pace,N.R. (2006) Bacterial RNase P: a new view of an ancient enzyme. *Nat. Rev. Microbiol.*, **4**, 729–740.
57. Stahley,M.R. and Strobel,S.A. (2005) Structural evidence for a two-metal-ion mechanism of group I intron splicing. *Science*, **309**, 1587–1590.
58. Yoshida,A., Shan,S., Herschlag,D. and Piccirilli,J.A. (2000) The role of the cleavage site 2′-hydroxyl in the *Tetrahymena* group I ribozyme reaction. *Chem. Biol.*, **7**, 85–96.